

Analysis of energy transfer in quantum networks using kinetic network approximations

David K. Moser^{1,2}

1: Department of Mathematics

2: Department of Physics

Northeastern University

Boston MA 02115

david.moser@gmx.net

November 13, 2018

Abstract

Coherent energy transfer in pigment-protein complexes has been studied by mapping the quantum network to a kinetic network. This gives an analytic way to find parameter values for optimal transfer efficiency. In the case of the Fenna-Matthews-Olson (FMO) complex, the comparison of quantum and kinetic network evolution shows that dephasing-assisted energy transfer is driven by the two-site coherent interaction, and not system-wide coherence. Using the Schur complement, we find a new kinetic network that gives a closer approximation to the quantum network by including all multi-site coherence contributions. Our new network approximation can be expanded as a series with contributions representing different numbers of coherently interacting sites.

For both kinetic networks we study the system relaxation time, the time it takes for the excitation to spread throughout the complex. We make mathematically rigorous estimates of the relaxation time when comparing kinetic and quantum network. Numerical simulations comparing the coherent model and the two kinetic network models, confirm our bounds, and show that the relative error of the new kinetic network approximation is several orders of magnitude smaller.

Keywords: exciton transfer, quantum efficiency, kinetic networks, FMO, coherent energy transfer, quantum networks, Schur complement.

Contents

1	Introduction	2
2	The quantum network	5
2.1	Master equation	5
2.2	Converting to vector equation	6
2.3	The coherent evolution matrix M	6
3	Kinetic networks	7
3.1	Extracting the kinetic network N	7
3.2	Expanding N	8
3.3	The network N_0	8
3.4	Including re-emission, recombination and trapping	9
3.5	Numerical simulations	10
4	Preliminaries	10
4.1	Norm	11
4.2	Conditions	11
4.3	Inverse bounds	12
4.4	Spectral properties	12

5	Bounding relaxation time error	13
5.1	Relaxation time	13
5.2	Resolvent difference	14
5.3	Comparing the relaxation time of M and N	14
5.4	Comparing the relaxation time of N and N_0	15
6	Bounding evolution error	16
6.1	Comparing the evolution of M and N	17
6.2	Comparing the evolution of N and N_0	18
7	Applications	19
7.1	Highly connected network	19
7.2	Linear network	20
7.3	The FMO-complex	21
8	Resolvent difference bounds	23
8.1	Bounds in the right half plane	23
8.2	Bounds parallel to the imaginary axis	25
9	Conclusion	26
10	Acknowledgments	26
A	Three sites	26
B	General construction	28
B.1	Constructing \tilde{a} and \tilde{b}_0	28
B.2	Constructing $\tilde{\nu}$	28
C	Calculations for applications	29
C.1	Highly connected network	29
C.2	Circular chain	30
	References	30

1 Introduction

Since coherent energy transfer in the Fenna-Matthews-Olson complex (FMO) has been observed [6, 9, 13], extensive experimental and theoretical research has been dedicated to studying coherent resonant transfer [5] and the coherent pigment-protein interaction [12, 8]. In particular, numerical solutions of simple models have shown that dephasing – the destruction of the coherences – at an intermediate rate helps to increase the energy transfer efficiency [10, 11]. This has been called dephasing- or environment-assisted energy transfer, and is analogous to a critically damped oscillator. The dephasing corresponds to damping and causes the exciton to relax to an equal distribution for every pigment site instead of staying localized due to the energy mismatch between the sites.

The models are based on two assumptions. First, only a single exciton is present, it is located at any of the seven pigments. The pigment exciton energy, and the pigment dipole-dipole interaction [4, 1] then lead to an oscillatory evolution of the system. And second, the site-environment interactions are assumed to be purely Markovian without any temporal or spatial correlations. The environment interactions are dephasing, recombination and trapping. Dephasing destroys the site coherences without destroying the exciton itself, and phonon recombination or photon re-emission lead to loss of the exciton to the environment. Trapping is the transfer of the exciton to the reaction center, where the electronic energy is converted to chemical energy, in FMO it occurs at pigment 3. The *transfer efficiency* is the probability that an exciton starting at site 1 or site 6 reaches the reaction center. For a general system with n pigments, we convert the master equation of the coherent model into vector form

$$\dot{\vec{\rho}} = M\vec{\rho}$$

where $\vec{\rho} \in \mathbb{R}^{n^2}$ is the density matrix in vector form and M is a real $n^2 \times n^2$ -matrix. Two procedures to find M are presented in 2.2 and 3.5.

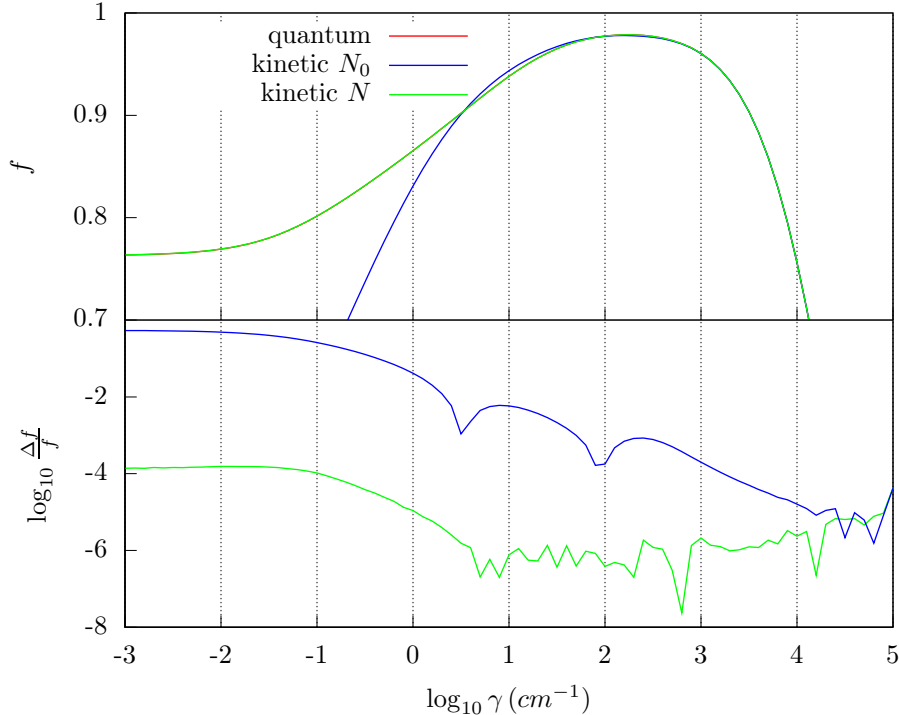


Figure 1: The efficiency of energy transfer in the FMO monomer. Model parameters are described in 7.3

To study population transfer channels and conditions for optimal transfer, a mapping to kinetic networks has been proposed [3, 7]. A kinetic network is a system where the exciton jumps incoherently between sites according to some fixed rates, i.e. a continuous-time Markov process. In its simplest version this approximation only takes into account the coherent interaction between pairs of sites to derive the transfer rate between them. If the two sites interact with strength V , have an energy separation E , and both sites experience dephasing at rate γ and population loss at rate κ then the rate is

$$\mu = \frac{2|V|^2(\gamma + \kappa)}{(\gamma + \kappa)^2 + E^2}. \quad (1)$$

This rate is maximized for the intermediate dephasing rate $\gamma = E - \kappa$ so the phenomenon of dephasing-assisted transfer is maintained in this approximation. For a system with n sites, these rates constitute the off-diagonals of a $n \times n$ rate matrix N_0 , and the system populations evolve according to

$$\dot{\vec{p}} = N_0 \vec{p}$$

where $\vec{p} \in \mathbb{R}^n$ is the time-dependent population vector. Figure 1 displays the transfer efficiency with models M and N_0 for different γ , the dephasing-assisted regime clearly shows as a peak around $\gamma \approx 170 \text{cm}^{-1}$. At the peak the population evolution of M is well approximated by that of N_0 , therefore dephasing-assisted energy transfer can be explained by the relatively simple coherent dynamic between pairs of sites that enters the rate μ and the influence of system-wide coherence is small.

To extract the limit of good approximation we introduce scaling variables, Γ which is proportional to the energy separations, dephasing and population loss rates, and Θ which is proportional to the site interactions. We will show that the approximation of N_0 to M becomes good as $\Theta\Gamma^{-1}$ approaches 0. We generalize the procedure of finding a kinetic network approximation in a mathematically appealing way using block matrices. We find a kinetic network matrix N that follows the evolution of M much closer – it is over three orders of magnitude more precise than the network N_0 as shown in Figure 1. Further, it can be expanded in $\Theta\Gamma^{-1}$ as

$$N = \sum_{k=0}^{\infty} N_k$$

where N_0 is the approximation described above, and the N_k are rate corrections due to coherent interactions via k intermediate sites. The expansion terms become smaller for increasing k , $N_k \propto \Theta \cdot (\Theta\Gamma^{-1})^k$. By stopping the expansion at a finite k kinetic networks approximation of varying accuracy can be formed allowing the study of coherent interaction at different “scales” or number of involved sites. We restrict our further investigation to the dominant contribution N_0 and the entire sum N .

In our exact bounds we study the system with all population-loss mechanisms removed. Due to dephasing the exciton spreads throughout the system at the *exciton relaxation time* τ and all populations become equal. The difference $\Delta\tau$ between relaxation times of M and N or N_0 gives a simple measure of how good the kinetic networks approximate the quantum network. As $\Theta\Gamma^{-1}$ becomes small the kinetic networks approach the quantum network and $\Delta\tau$ becomes small as well.

We define τ and $\Delta\tau$ as follows, using the Euclidean norm $\|\vec{p}\|_2 = \sqrt{\sum_{i=1}^n p_i^2}$ to compare population vectors.

Definition 1.

1. The map $T : \mathbb{R}^{n^2} \rightarrow \mathbb{R}^n$ is the restriction of density vectors $\vec{\rho}$ to population vectors \vec{p} , and consequently T^\dagger gives the embedding of population vector space in density vector space. In particular, if the first n components of $\vec{\rho}$ represent the site populations, then $T = (\mathbb{1}_n, 0_{n \times (n^2-n)})$.

2. The maximum relaxation time is

$$\tau = \max_{\vec{p}_0} \left\| \int_0^\infty e^{Nt} \vec{p}_0 - \frac{1}{n} dt \right\|_2$$

and the corresponding minimal relaxation rate is

$$\mu = \frac{1}{\tau}$$

3. The maximum deviation of relaxation time between the quantum network M and the kinetic network N is

$$\Delta\tau = \max_{\vec{p}_0} \left\| \int_0^\infty (Te^{Mt}T^\dagger - e^{Nt}) \vec{p}_0 dt \right\|_2.$$

4. Define τ_0 , μ_0 and $\Delta\tau_0$ in the same way, replacing N with N_0 .

For our bounds we require that every site experiences dephasing. Further, the network has to be *connected*, meaning that any two sites can exchange populations -directly or indirectly- such that the relaxed state will have equal population everywhere. And finally we also require our site interactions to be real – but it is clear from our proofs that the generalization to complex interactions could be treated in a similar manner.

Our first results shows how fast the relaxation time of the two kinetic networks N_0 and N approximate that of the quantum network M as $\Theta\Gamma^{-1}$ gets small.

Theorem 2. *There are scaling invariant constants k_1 and k_2 , such that for $\Theta\Gamma^{-1}$ small enough we have the following bounds:*

1. *The relative difference of relaxation time between quantum evolution M and kinetic evolution N_0 is bounded by*

$$\Delta\tau_{0,\text{rel}} = \Delta\tau_0/\tau_0 \leq k_1\Theta\Gamma^{-1}.$$

2. *The relative difference of relaxation time between quantum evolution M and kinetic evolution N is bounded by*

$$\Delta\tau_{\text{rel}} = \Delta\tau/\tau \leq k_2\Theta^2\Gamma^{-2}.$$

This Theorem follows from Theorem 5 and Corollary 7 in Section 5.

We also find the following exponential bounds on the time dependence.

Theorem 3. *There are scaling invariant constants k_3 , k_4 and k_5 , such that for any initial population distribution \vec{p}_0 we have the following bounds, as long as $\Theta\Gamma^{-1}$ is small enough:*

1. *For all times $t \geq 0$*

$$\|Te^{Mt}T^\dagger\vec{p}_0 - e^{N_0t}\vec{p}_0\|_2 \leq k_3e^{-\mu_0t/2} \cdot \Theta\Gamma^{-1}.$$

2. *For all times $t \geq 0$*

$$\|Te^{Mt}T^\dagger\vec{p}_0 - e^{Nt}\vec{p}_0\|_2 \leq k_4e^{-\mu t/2} \cdot \Theta^2\Gamma^{-2}(1 + k_5 \log \Theta\Gamma^{-1}).$$

This Theorem follows from Theorem 8 and Corollary 10 in Section 6. We expect that more sophisticated methods might yield the same bound without the $\Theta^2\Gamma^{-2} \log \Theta\Gamma^{-1}$ term.

2 The quantum network

We first introduce the Master equation for the coherent model. Then we reformulate the equation in vector form and combine the entire dynamic in the real $n^2 \times n^2$ -matrix M . We describe the general structure of M as a preparation to the next section, where we generate kinetic networks from parts of M .

2.1 Master equation

We consider the same quantum mechanical system studied in [11] with n sites carrying a single excitation which is equivalent to a system with n states/levels. The site energies are $E_k \in \mathbb{R}$ so the energy operator is

$$H = \sum_{k=1}^n E_k |k\rangle\langle k|.$$

The site k couples to site l with interaction strength $V_{kl} \in \mathbb{C}$ so the interaction operator is

$$V = \sum_{k \neq l} V_{kl} |k\rangle\langle l|$$

where $V_{kl} = \overline{V_{lk}}$. Site trapping, re-emission and recombination can be incorporated by an anti-hermitian operator A . Let κ_k be the combined rate of exciton loss at site k due to these effects, then A is defined as

$$A = \frac{-i}{2} \sum_{k=1}^n \kappa_k |k\rangle\langle k|.$$

Finally, every site is also under the influence of dephasing at rate $\gamma_k \geq 0$ incorporated in the Lindbladian superoperator

$$\mathcal{L}(\rho) = \sum_{k=1}^n L_k \rho L_k^\dagger - \frac{1}{2} \{\rho, L_k^\dagger L_k\}$$

with $L_k = \sqrt{\gamma_k} |i\rangle\langle i|$. Setting $\hbar = 1$, the single exciton manifold of the quantum network is described by the master equation

$$\dot{\rho} = -i[H + V, \rho] - i\{A, \rho\} + \mathcal{L}(\rho) \quad (2)$$

where square and curly brackets represent commutator and anti-commutator respectively.

For now we set $A = 0$, ignoring exciton depleting processes as explained above. We will mention how to include them in the kinetic network approximations later on. Our approximation becomes exact in the limit where the energy difference between sites is large, the dephasing is large and the interactions are small. To be specific, we introduce scaling parameters Γ and Θ and consider the limit $\Theta\Gamma^{-1} \rightarrow 0$. Energies and dephasing scale like Γ and interactions scale like Θ

$$\begin{aligned} E_k &\propto \Gamma, \\ \gamma_k &\propto \Gamma, \\ V_{kl} &\propto \Theta. \end{aligned}$$

With these assumptions the master equation turns into

$$\dot{\rho} = -i[\Gamma H + \Theta V, \rho] + \Gamma \mathcal{L}(\rho). \quad (3)$$

Because this equation is linear in ρ it can be converted into vector form

$$\dot{\vec{\rho}} = M \vec{\rho}$$

where $\vec{\rho} \in \mathbb{R}^{n^2}$ is the density matrix in vector form and M is a real $n^2 \times n^2$ -matrix. Two procedures to find M are presented in 2.2 and 3.5.

2.2 Converting to vector equation

We rewrite the master equation (3), skipping the scaling factors Θ and Γ , it is easy to reintroduce them at a later point

$$\dot{\rho} = -i[H + V, \rho] + \mathcal{L}(\rho). \quad (4)$$

Our first goal is to convert this into the differential equation

$$\dot{\vec{\rho}} = M\vec{\rho}$$

for density “vectors” $\vec{\rho} \in \mathbb{R}^{n^2}$. Notice that because $\rho = \rho^\dagger$ the space of density matrix has n^2 real dimensions, so we are not using any information when mapping ρ to $\vec{\rho}$.

We use the following conversion:

1. The first n entries of the density vector are the populations – the real diagonal entries of ρ .
2. For the entries $n + 1$ to n^2 we alternate between real and imaginary parts of the coherences – the off-diagonal entries of ρ – starting with entry ρ_{kl} where $k = 1$ and $l = 2$ continuing by increasing l until $l = n$, then moving to the entry ρ_{23} . We multiply all these entries with $\sqrt{2}$, a normalization factor useful to achieve simpler expressions later on.

In terms of index equations this is:

1. For $k = 1 \dots n$

$$\vec{\rho}_k = \rho_{kk}.$$

2. For $k, l \in \{1, \dots, n\}$ with $k < l$

$$\begin{aligned} \vec{\rho}_{n+2n(k-1)-k(k+1)+2l-1} &= \sqrt{2} \operatorname{Re} \rho_{kl} \\ \vec{\rho}_{n+2n(k-1)-k(k+1)+2l} &= \sqrt{2} \operatorname{Im} \rho_{kl}. \end{aligned}$$

Other mappings will yield the same kinetic networks, as long as they allow for an easy separation of population and coherence space.

While somewhat tedious, it is now relatively straightforward to find the matrix M such that

$$\dot{\vec{\rho}} = M\vec{\rho}.$$

To find the rows $k = 1 \dots n$ we write out the diagonal components of the RHS of (4), and to find rows $k = n+1, \dots, n^2$ we write out the off-diagonals of the RHS of (4). We follow this procedure explicitly for the case $n = 3$ in Appendix A. From there it is obvious how the procedure generalizes to larger n . Here we will only present the final form.

2.3 The coherent evolution matrix M

For simple notation and to simply extract the kinetic networks we split up the density vector space \mathbb{R}^{n^2} . Let $P = \mathbb{R}^n$ be the space of populations and let $C = \mathbb{R}^{n^2-n}$ be the space of coherences. We can then write density vectors as $\vec{\rho} = \begin{pmatrix} \vec{p} \\ \vec{c} \end{pmatrix}$ with $\vec{p} \in P$ and $\vec{c} \in C$. With this splitting the matrix M describing the quantum network looks like

$$M = \begin{pmatrix} 0 & -a^\dagger \\ a & b \end{pmatrix}$$

where $a : P \rightarrow C$ and $b : C \rightarrow C$ are real matrices (so $a^\dagger = a^\top$, but we’ll keep the more general notation for later). Notice that the populations do not affect each other directly, but only via the coherences.

Matrix a describes how populations couple to coherences, its entries are real and imaginary parts of V_{kl} , naturally, site k will only couple to coherences kl with $l \neq k$, thus of the $(n^2 - n)$ entries in the k -th column of a only $2(n - 1)$ are nonzero. Matrix b describes how coherences couple to other coherences, if considered as a block matrix with 2×2 -blocks the diagonal block for the coherence between site k and site l is of the form

$$\begin{pmatrix} -\gamma_{kl} & -E_{kl} \\ E_{kl} & -\gamma_{kl} \end{pmatrix} \quad (5)$$

where

$$\begin{aligned}\gamma_{kl} &= \frac{1}{2}(\gamma_k + \gamma_l) \\ E_{kl} &= E_k - E_l.\end{aligned}$$

The off-diagonal blocks consist of real and imaginary parts of V_{kl} .

From the form of M , when ignoring the off-diagonal blocks of b , we see that the site k couples to the site l via the coupling strength V_{kl} , then some mixture of γ_{kl} and E_{kl} and then again via the coupling strength V_{kl} . This reminds us of the rates of the form $\mu = \frac{2V^2\gamma}{\gamma^2 + E^2}$ described in (1) that make up the matrix N_0 . We will make this intuition precise in the next subsections.

3 Kinetic networks

In this section we show how the kinetic network N emerges naturally out of the study of the resolvent $(z - M)^{-1}$. We expand N in powers of $\Theta\Gamma^{-1}$, giving the series

$$N = \sum_{k=0}^{\infty} N_k$$

with the leading order contribution being N_0 . For some steps involving matrix calculations we only give a simplified version. However, in Appendix (A) we follow the procedure described below, giving the full expressions in the case $n = 3$.

3.1 Extracting the kinetic network N

To extract kinetic networks from M we consider its resolvent $(z - M)^{-1}$. Remember that for any holomorphic function f we have

$$f(M) = \frac{1}{2\pi i} \oint f(z)(z - M)^{-1} dz.$$

Therefore, if one can bound the resolvent appropriately, one can also bound the evolution operator e^{Mt} and other related quantities. Because we only care about approximating the population dynamics we restrict our view to the population block of the resolvent of M . The Banchiewicz formula [2] gives the inverse of a 2×2 -block matrix. The first block of the inverse – in our case the population block – is called the Schur complement, and due to its basic nature has many applications in applied mathematics, statistics and physics [14]. Here we use it to “pull” the coherence dynamic back into population space. Only writing the Schur complement and skipping the other blocks of the resolvent we have

$$(z - M)^{-1} = \begin{pmatrix} (z - a^\dagger(b - z)^{-1}a)^{-1} & \cdot \\ \cdot & \cdot \end{pmatrix}.$$

Remember the operator T , the restriction to population space. With our choice of density vector basis it has the form

$$T = \begin{pmatrix} \mathbb{1}_n & 0_{n \times (n^2 - n)} \end{pmatrix}.$$

The difference of evolution for initial conditions $\vec{\rho}_0 = \begin{pmatrix} \vec{p}_0 \\ 0 \end{pmatrix} = T^\dagger \vec{p}_0$ (zero coherences) between quantum network M and kinetic network N is thus

$$(Te^{Mt}T^\dagger - e^{Nt})\vec{p}_0 = \frac{1}{2\pi i} \oint e^{zt} ((z - a^\dagger(b - z)^{-1}a)^{-1} - (z - N)^\dagger) dz.$$

For a good approximation we require

$$(z - a^\dagger(b - z)^{-1}a)^{-1} \approx (z - N)^\dagger. \quad (6)$$

At this point it is a small step to drop the second z on the LHS, in which case the formula becomes equality if we set

$$N = a^\dagger b^{-1} a.$$

To see intuitively that this approximation is good, consider the following. Matrix b contains terms proportional to Γ on its diagonal and terms proportional to Θ on its off-diagonal, matrix a is proportional to Θ , therefore

$$N \propto \Theta^2 \Gamma^{-1}$$

when $\Theta \Gamma^{-1}$ becomes small. For values of z that are smaller than eigenvalues of b the approximation (6) is good because $(b - z)^{-1} \approx b^{-1}$, for values of z larger than eigenvalues of b is good, because then z is much larger than the eigenvalues of N , and so both sides of (6) are approximately z^{-1} . This basic insight is what drives our bounds in Section 8.

3.2 Expanding N

As mentioned in 2.3, b consists of 2×2 -blocks proportional to Γ on the diagonal and 2×2 -blocks proportional to Θ on the off-diagonal. We separate this contributions defining

$$b = b_0 + \nu$$

where $b_0 \propto \Gamma$ and $\nu \propto \Theta$ is the block-diagonal and block-off-diagonal of b respectively. If $\Theta \Gamma^{-1}$ is small enough and if b_0 is invertible we can expand

$$b^{-1} = \sum_{k=0}^{\infty} b_0^{-1} (-\nu b_0^{-1})^k .$$

This leads to the expansion

$$N = a^\dagger b^{-1} a = \sum_{k=0}^{\infty} N_k$$

with

$$N_k = a^\dagger b_0^{-1} (-\nu b_0^{-1})^k a . \quad (7)$$

When using explicit forms of a , b_0 and ν one can see that the rates in N_k consist of corrections due to interactions via k intermediates. Roughly speaking, every of the $(k + 1)$ sites along the chain contributes a factor of Θ , every of the k coherences (links) contributes a factor of Γ^{-1} , thus N_k scales like $\Theta^{k+1} \Gamma^{-k}$.

3.3 The network N_0

We now present the explicit form of

$$N_0 = a^\dagger b_0^{-1} a$$

the dominant contribution to N . We only show the crucial parts of the calculations that should make clear how to get the result for general n .

Notice that, from 3.2 and (5), it follows that b_0 is a $(n^2 - n) \times (n^2 - n)$ matrix with the only nonzero entries being 2×2 blocks

$$\begin{pmatrix} -\gamma_{kl} & -E_{kl} \\ E_{kl} & -\gamma_{kl} \end{pmatrix}$$

along the diagonal. With the unitary transformation

$$U_0 = \frac{1}{\sqrt{2}} \begin{pmatrix} -i & i \\ 1 & 1 \end{pmatrix}$$

we can diagonalize these 2×2 blocks. Hence, the entire matrix b_0 can be diagonalized by applying the transformation

$$U = \mathbb{1}_{(n^2-n)/2} \otimes U_0 \quad (8)$$

and

$$\tilde{b}_0 = U^\dagger b_0 U = \text{diag}(\alpha_{12}, \bar{\alpha}_{12}, \alpha_{13}, \bar{\alpha}_{13}, \dots, \bar{\alpha}_{n-1,n}) \quad (9)$$

with

$$\alpha_{kl} = -\gamma_{kl} + iE_{kl}$$

where diag denotes a diagonal matrix with given diagonal entries. In fact, U also helps to simplify a , consider the case $n = 3$

$$\tilde{a} = U^\dagger a = \begin{pmatrix} \bar{V}_{12} & -\bar{V}_{12} & \\ V_{12} & -V_{12} & \\ \bar{V}_{13} & & -\bar{V}_{13} \\ V_{13} & & -V_{13} \\ & \bar{V}_{23} & -\bar{V}_{23} \\ & V_{23} & -V_{23} \end{pmatrix}, \quad (10)$$

and the same happens for $\tilde{\nu} = U^\dagger \nu U$ (derivation in Appendix A). Notice that both \tilde{b}_0 and \tilde{a} are complex matrices, still, we can use the transformed matrices \tilde{a} , \tilde{b}_0 , and $\tilde{\nu}$ when finding explicit expressions for the real matrices N_k , because U cancels out. For example

$$\begin{aligned} N_0 &= a^\dagger b_0^{-1} a \\ &= a^\dagger U U^\dagger b_0^{-1} U U^\dagger a. \\ &= (U^\dagger a)^\dagger (U^\dagger b_0^{-1} U)^{-1} (U^\dagger a) \\ &= \tilde{a}^\dagger \tilde{b}_0^{-1} \tilde{a}. \end{aligned}$$

In the case $n = 3$ we get

$$N_0 = \begin{pmatrix} -\mu_{12} - \mu_{13} & \mu_{12} & \mu_{13} \\ \mu_{12} & -\mu_{12} - \mu_{23} & \mu_{23} \\ \mu_{13} & \mu_{23} & -\mu_{13} - \mu_{23} \end{pmatrix} \quad (11)$$

with

$$\mu_{kl} = \frac{2|V_{kl}|^2 \gamma_{kl}}{\gamma_{kl}^2 + E_{kl}^2}.$$

The following simplified calculation illustrates how the rates μ_{kl} result from the matrix multiplication $\tilde{a}^\dagger \tilde{b}_0^{-1} \tilde{a}$

$$\begin{aligned} \begin{pmatrix} \bar{V} \\ V \end{pmatrix}^\dagger \begin{pmatrix} \alpha^{-1} & 0 \\ 0 & \bar{\alpha}^{-1} \end{pmatrix} \begin{pmatrix} -\bar{V} \\ -V \end{pmatrix} &= -V\bar{V}(\alpha^{-1} + \bar{\alpha}^{-1}) \\ &= \frac{2|V|^2 \gamma}{\gamma^2 + E^2}. \end{aligned}$$

More generally for any n we have

$$(N_0)_{kl} = \mu_{kl} \quad (12)$$

for $i \neq j$ and

$$(N_0)_{kk} = -\sum_{l \neq k} \mu_{kl} \quad (13)$$

This is just the network described in [3] and the introduction.

3.4 Including re-emission, recombination and trapping

The population decreasing effects of re-emission, recombination and trapping can all be described by the rates κ_k of the diagonal anti-hermitian operator

$$A = \frac{-i}{2} \sum_{k=1}^n \kappa_k |k\rangle \langle k|$$

included in our general master equation (2). The contribution to the rate of change $\dot{\rho}$ is easily calculated

$$-i\{A, \rho\} = -\sum_{k,l} \frac{1}{2} (\kappa_k + \kappa_l) |i\rangle \langle j|,$$

and M becomes

$$M = \begin{pmatrix} c_1 & -a^\dagger \\ a & b + c_2 \end{pmatrix}$$

with the new contributions

$$c_1 = -\text{diag}(\kappa_1, \kappa_2, \dots, \kappa_n)$$

and

$$c_2 = -\text{diag}(\kappa_{12}, \kappa_{12}, \kappa_{13}, \kappa_{13}, \dots, \kappa_{n-1,n})$$

with $\kappa_{kl} = \frac{1}{2}(\kappa_k + \kappa_l)$ the rate that decreases the coherence of sites k and l . With this the networks become

$$\begin{aligned} N_0 &= a^\dagger (b_0 + c_2)^{-1} a + c_1 \\ N &= a^\dagger (b + c_2)^{-1} a + c_1 \\ N_k &= a^\dagger (b_0 + c_2)^{-1} (-\nu(b_0 + c_2)^{-1})^k a \end{aligned} \quad (14)$$

which also hold with the replacements $a \rightarrow \tilde{a}$, $b \rightarrow \tilde{b}$ and $\nu \rightarrow \tilde{\nu}$, while leaving c_1 and c_2 unchanged.

The rates in N_0 can again be calculated directly

$$(N_0)_{kl} = \mu_{kl} = \frac{2 |V_{kl}|^2 (\gamma_{kl} + \kappa_{kl})}{(\gamma_{kl} + \kappa_{kl})^2 + E_{kl}^2}$$

for $k \neq l$ and

$$(N_0)_{kk} = -\kappa_k - \sum_{l \neq k} \mu_{kl}.$$

3.5 Numerical simulations

According to the last two subsections, network N_0 is easy to calculate directly, while network N and any k -site contribution N_k can be formed from the general definition of \tilde{a} , \tilde{b}_0 and $\tilde{\nu}$ (see Appendix (B)) which can be somewhat tedious. However, there is another approach related to numerical simulations. When running numerical calculations to simulate a complex master equation (2) on a software like Octave or Matlab, the need to convert the equation to the form

$$\dot{\vec{\rho}} = M \vec{\rho}$$

with a real M arises in any case. This can be done as we describe it in 2.2, or more easily – because we have the help of a computer – by defining an orthonormal density space basis. For example set

$$\begin{aligned} \sigma_k &= |k\rangle\langle k| \\ \xi_{kl} &= (|k\rangle\langle l| + |l\rangle\langle k|)/\sqrt{2} \\ \eta_{kl} &= (-i|k\rangle\langle l| + i|l\rangle\langle k|)/\sqrt{2} \end{aligned}$$

for $k < l$. Then matrix M can be formed by applying the master equation to those vectors and finding their coordinates. The following gives the population space block of M

$$M_{kl} = \text{Tr} \left(\sigma_k^\dagger \mathcal{M}(\sigma_l) \right)$$

where \mathcal{M} is the superoperator formed by the RHS of the master equation (2). Once the entire real matrix is found it is cut into population and coherence blocks

$$M = \begin{pmatrix} m_{PP} & m_{PC} \\ m_{CP} & m_{CC} \end{pmatrix}$$

and a generalized kinetic network of the same form as N is calculated as

$$N = m_{PC} m_{CC}^{-1} m_{CP} + m_{PP}.$$

Hence, if one has already calculated M in order to simulate a quantum network, it only takes a few steps to find the kinetic network approximation N .

4 Preliminaries

In this section we give some definitions and conditions. The conditions allow us to infer basic facts about the spectra of the operators N_0 , N and M , which are required for all our bounds in Sections (5), (6) and (8).

4.1 Norm

Because for our bounds of the relaxation time we remove all population decreasing effects all evolutions M , N_0 , and N leave the total population invariant. Therefore we split up the space of populations P . Set

$$\vec{e} = (1, 1, \dots, 1)^\dagger / n \in P$$

the equal population vector. As we will prove in Proposition 4, as long as the network meets certain conditions, both quantum and kinetic evolutions will tend to \vec{e} for any initial condition with total population 1. Consequently, we are only interested in the properties of our matrices in the space of population inequalities

$$I = \vec{e}^\top = \left\{ \vec{v} \left| \sum_k v_k = 0 \right. \right\}.$$

This is reflected in the norm we use, defines as follows. For $A : X_1 \rightarrow X_2$ where X_1 and X_2 are equal to I or C we define the operator norm as

$$\|A\| = \sup_{v \in X_1} \frac{\|Av\|_2}{\|v\|_2}$$

where $\|\cdot\|_2$ is the Euclidean norm. Hence, from now on, we think of our matrix blocks as

$$\begin{aligned} a &: I \rightarrow C \\ b &: C \rightarrow C \\ a^\dagger &: C \rightarrow I. \end{aligned}$$

Note that $\|a\|$ is the same if we maximize over I or P because $a\vec{e} = 0$, and that $\|a\| = \|a^\dagger\|$. Also, according to Proposition 4 $N_0 < 0$ on I and therefore N_0^{-1} is well-defined. The same holds for N . Define

$$\mu = \|N^{-1}\|^{-1}$$

to be the eigenvalue closest to 0 in N in I , define μ_0 the same way for N_0 .

4.2 Conditions

For all our following bounds we have a set of conditions.

- First, we require that the network is *connected*, in the sense that any two sites k and l are coupled, at least via some intermediates, i.e. for some integer $p \geq 0$ there are sites m_j , $j = 1 \dots p$ such that the product

$$V_{km_1} V_{m_1 m_2} \dots V_{m_{p-1} m_p} V_{k_p j}$$

is nonzero. This condition ensures that all sites can exchange population and the evolution ultimately converges to \vec{e} .

- Second, we require all the site dephasing rates to be strictly positive, $\gamma_k > 0$. This condition is essential for our approximation, as the coherences need to decay for the evolution M to become non-oscillatory. Notice that the limit $\Theta\Gamma^{-1} \rightarrow 0$ does not require that the dephasing rates get larger, but they will be much larger than the magnitude of eigenvalues of N or N_0 , the population decay rates, because $\Gamma \gg \Theta^2\Gamma^{-1}$.
- Finally, we require that the V_{kl} are *real*. This ensures that N is symmetric and has a real spectrum (see Proposition 4), which allows simpler bounds in our proofs. While N_0 is always symmetric, we first compare the evolutions of M and N , and then the evolutions of N and N_0 . Therefore we require this condition for both N_0 and N . We are confident that our methods would extend to the case of complex V_{kl} , but for the sake of clarity we restrict ourselves to the simpler case.

4.3 Inverse bounds

Our proofs consist mainly of using the following two bounds on the inverse on different parts of resolvents.

First, consider the Taylor series of the inverse close to 1, which for real numbers x gives

$$|(1+x)^{-1} - 1| \leq 2|x|$$

for $|x| \leq 1/2$. This is readily translated to a bound for operators

$$\|(A+B)^{-1} - A^{-1}\| \leq 2 \|A^{-1}\|^2 \|B\| \quad (15)$$

for $\|B\| \leq \frac{1}{2} \|A^{-1}\|^{-1}$.

Second, if $A < -c < 0$ is a negative definite, self-adjoint, finite dimensional operator and $z \in \mathbb{C}$ with $\operatorname{Re} z \geq 0$ then

$$\|(z-A)^{-1}\| \leq c^{-1} \quad (16)$$

and

$$\|(z-A)^{-1}\| \leq |z|^{-1}. \quad (17)$$

these two bounds follow from the fact

$$\begin{aligned} \|(z-A)^{-1}\| &= \max \{ |\lambda| \mid \lambda \in \operatorname{Spec}(z-A)^{-1} \} \\ &= \max \{ |(z-\lambda)^{-1}| \mid \lambda \in \operatorname{Spec} A \}. \end{aligned}$$

4.4 Spectral properties

The following Proposition gives some basic facts about the spectra of the kinetic networks N and N_0 . We will use these properties for the proofs of our bounds.

Proposition 4. *The matrices N_0 and N as defined in 3.3 and 3.1 have the following properties*

1. N_0 is real and symmetric.
2. N is real.
3. If the interactions V_{kl} are real then N is symmetric.
4. $N_0 \vec{e} = N \vec{e} = 0$
5. If $\gamma_k > 0$ and the network is connected network then $N_0 < 0$ on I .
6. For $\Theta \Gamma^{-1}$ small enough, $N_0 < -\mu/2$ and $N < -\mu_0/2$ on I .

Proof. 1. These properties follow directly from the form in (12) and (13).

2. N is real because it is a product of a , b^{-1} and a^\dagger which are also real.

3. If V_{kl} is real then \tilde{a} (see (10)) is real, so

$$N = \tilde{a}^\top \tilde{b}^{-1} \tilde{a}$$

Furthermore, $\tilde{b}^\top = \tilde{b}$ (see Appendix A) therefore

$$\begin{aligned} N^\top &= \tilde{a}^\top \left(\tilde{b}^{-1} \right)^\top \tilde{a} \\ &= \tilde{a}^\top \left(\tilde{b}^\top \right)^{-1} \tilde{a} \\ &= N. \end{aligned}$$

4. From (10) it is not hard to understand how \tilde{a} looks for any n . One sees that the two rows for the coherence between sites k and l have exactly two non-zero entries, the first has V_{kl} and $-V_{kl}$, and the second has \bar{V}_{kl} and $-\bar{V}_{kl}$. Therefore $\tilde{a} \vec{e} = 0$ and so $N_0 \vec{e} = N \vec{e} = 0$.

5. For $\vec{v} \in I$ we have $\sum_k v_k = 0$. Now

$$\begin{aligned} \vec{v}^\dagger N_0 \vec{v} &= - \sum_{k < l} \mu_{kl} (v_k - v_l)^2 \\ &\leq 0 \end{aligned}$$

The condition for equality is as follows. Because $\gamma_k > 0$ we have

$$V_{kl} \neq 0 \iff \mu_{kl} \neq 0.$$

Hence, because the network is connected, we have $v_k = v_l$ for all k and l and with $\sum_k v_k = 0$ it follows that $\vec{v} = 0$, thus $N_0 < 0$ on I .

6. Because $\mu_0 = \|N_0^{-1}\|^{-1}$ and $N_0 < 0$ we have $N_0 \leq -\mu_0$ on I . Note that $\mu \propto \Theta^2 \Gamma^{-1}$ can grow as $\Theta \Gamma^{-1}$ gets small, so $\mu - \mu_0$ can grow in absolute value, however, as we now show the spectra of N and N_0 approach each other relative to their “size”

$$\mu - \mu_0 \ll \mu_0$$

We bound the distance of N and N_0 with the inverse bound. For $\Theta \Gamma^{-1}$ small enough we have $\|\nu\| \leq \frac{1}{2} \|b_0^{-1}\|^{-1}$ and we can apply (15) on

$$\|(b_0 + \nu)^{-1} - b_0^{-1}\| \leq 2 \|b_0^{-1}\|^2 \|\nu\|.$$

Now

$$\begin{aligned} \|N - N_0\| &= \|a^\dagger (b^{-1} - b_0^{-1}) a\| \\ &= \|a\|^2 2 \|b_0^{-1}\|^2 \|\nu\|. \end{aligned}$$

So, the distance of N and N_0 is proportional to $\Theta^2 \Gamma^{-2} \Theta$, and the eigenvalues in N_0 and N – in particular μ_0 and μ – are proportional to $\Theta^2 \Gamma^{-1}$. Comparing the two gives

$$\Theta^2 \Gamma^{-2} \Theta \ll \Theta^2 \Gamma^{-1}$$

because $\Theta \Gamma^{-1} \ll 1$. That means the eigenvalues are approaching each other relative to their magnitude, in particular N becomes negative definite like N_0 , and

$$\frac{|\mu - \mu_0|}{\mu_0} \rightarrow 0.$$

Now it immediately follows that

$$\begin{aligned} N &< -\mu < \mu_0/2 \\ N_0 &< -\mu_0 < \mu/2. \end{aligned}$$

□

5 Bounding relaxation time error

We now give an explicit definition of relaxation time and the norms we use to control it. Then we derive bounds first comparing the quantum network M to the kinetic network N , and then comparing the kinetic networks N and N_0 .

As a simple check of sanity consider the following. If we scale $\Gamma \propto s$ and $\Theta \propto s$ then also $M, N \propto s$ and time scales inversely $\Delta\tau, \tau \propto s^{-1}$. Therefore the relative error $\Delta\tau_{\text{rel}} = \Delta\tau/\tau$ stays unchanged and we expect bounds in terms of positive powers of $\Theta \Gamma^{-1}$. Our two bounds show exactly this behavior. The approximation of N to M is proportional to $\Theta^2 \Gamma^{-2}$, while the approximation of N_0 to N is proportional to $\Theta \Gamma^{-1}$, combining the two approximations it follows that the approximation of N_0 to M is also proportional $\Theta \Gamma^{-1}$.

Note that all the results in this Section require the conditions in 4.2.

5.1 Relaxation time

By Proposition (4), the eigenvalues of N and N_0 on I are all negative for $\Theta \Gamma^{-1}$ small enough, so for any initial distribution $\vec{p}_0 \in I$

$$\begin{aligned} e^{Nt} \vec{p}_0 &\rightarrow 0 \\ e^{N_0 t} \vec{p}_0 &\rightarrow 0 \end{aligned}$$

for large t . We can integrate

$$\int_0^\infty e^{Nt} dt = N^{-1}$$

and applying the operator norm maximizes the relaxation time for the kinetic network N over all possible population inequalities $\vec{p}_0 \in I$, set

$$\begin{aligned} \tau &= \mu^{-1} = \|N^{-1}\| = \|(a^\dagger b^{-1} a)^{-1}\| \\ &= \left\| \int_0^\infty e^{Nt} dt \right\| \end{aligned}$$

and in the same way we define $\tau_0 = \mu_0^{-1}$ for the network N_0 .

We define the error in relaxation time as the relaxation time difference maximized over I

$$\Delta\tau = \left\| \int_0^\infty T e^{Mt} T^\dagger - e^{Nt} dt \right\|.$$

Hence, bounding $\Delta\tau$ means controlling the *worst possible* error in relaxation time when approximating M by N . The relative error is

$$\Delta\tau_{\text{rel}} = \Delta\tau/\tau$$

notice that we compare the worst possible relaxation time error to the longest possible relaxation time, those two do not necessarily occur for the same initial condition. We define $\Delta\tau_0$ and $\Delta\tau_{0,\text{rel}}$ in the same way, comparing N and N_0 .

5.2 Resolvent difference

Converting the operator for the relaxation time error we get

$$\begin{aligned} \int_0^\infty T e^{Mt} T^\dagger - e^{Nt} dt &= T M^{-1} T^\dagger - N^{-1} \\ &= \frac{1}{2\pi i} \oint \frac{1}{z} \left(T \frac{1}{z-M} T^\dagger - \frac{1}{z-N} \right) dz \\ &= \frac{1}{2\pi i} \oint \frac{1}{z} \left(\frac{1}{z - a^\dagger(b-z)^{-1}a} - \frac{1}{z - a^\dagger b^{-1}a} \right) dz, \end{aligned}$$

where the complex integration follows a contour surrounding both $\text{Spec } M$ and $\text{Spec } N$. Define $S(z)$ to be the difference of the two resolvents

$$S(z) = \frac{1}{z - a^\dagger(b-z)^{-1}a} - \frac{1}{z - a^\dagger b^{-1}a}.$$

We now seek a bound on

$$\left\| \int_0^\infty T e^{Mt} T^\dagger - e^{Nt} dt \right\| = \left\| \frac{1}{2\pi i} \oint \frac{1}{z} S(z) dz \right\|. \quad (18)$$

5.3 Comparing the relaxation time of M and N

When bounding second order terms with the inverse bound we encounter

$$\kappa = \|a\|^2 \|b^{-1}\|^2$$

and κ_0 for the corresponding terms with b_0 instead of b . Notice the scaling behavior $\mu, \mu_0 \propto \Theta^2 \Gamma^{-1}$ and $\kappa, \kappa_0 \propto \Theta^2 \Gamma^{-2}$.

We will change the contour integration in (18) to be along the imaginary axis $z = iy$ for $y \in \mathbb{R}$. We prove the somewhat technical bounds on $S(iy)$ in Lemma 11 in Section 8.

Theorem 5. *If $\Theta \Gamma^{-1}$ is small enough then*

$$\Delta\tau = \left\| \int_0^\infty T e^{Mt} T^\dagger - e^{Nt} dt \right\| \leq \frac{4}{\pi} \kappa \mu^{-1} (1 + \beta)$$

where $\beta > 0$ is the scaling independent constant from Lemma 11. This gives a bound on the relative error

$$\Delta\tau_{\text{rel}} = \Delta\tau/\tau \leq \frac{4}{\pi}\kappa(1 + \beta) = k_2\Theta^2\Gamma^{-2}$$

where k_2 is scaling invariant.

Proof. We set the integration contour in (18) to be along the complex axis $z = iy$ for $y \in \mathbb{R}$ with y going from $-R$ to $+R$. We close the contour to the left in the half plane of negative real parts along a circle of radius R . According to Lemma 11, $S(z)$ has no poles with $\text{Re } z \geq 0$ and so all poles lie within this contour for R large enough and $\Theta\Gamma^{-1}$ small enough. As R tends to infinity the integrand behaves like $\frac{1}{z^3}$ so the half-circle does not contribute to the integral. We can therefore change to complex integral to an integral in y over all of \mathbb{R}

$$\left\| \int_0^\infty T e^{Mt} T^\dagger - e^{Nt} dt \right\| = \left\| \frac{1}{2\pi} \int_{\mathbb{R}} \frac{1}{iy} S(iy) dy \right\|.$$

Now split up the integral into two regions $|y| \leq \mu$ and $|y| \geq \mu$ and then use the corresponding bounds from Lemma 11. Choose $\Theta\Gamma^{-1}$ small enough so that $\mu < \alpha$ and use part 1 of the Lemma to bound

$$\begin{aligned} \left\| \int_{-\mu}^\mu \frac{1}{iy} S(iy) dy \right\| &\leq \int_{-\mu}^\mu \frac{1}{|y|} \cdot 4\kappa\mu^{-2}|y| dy \\ &\leq 8\kappa\mu^{-1}, \end{aligned}$$

and use part 2 of the Lemma to bound

$$\begin{aligned} \left\| \int_\mu^\infty \frac{1}{iy} S(iy) dy \right\| &\leq \int_\mu^\infty \frac{1}{|y|} \cdot 4\beta\kappa|y|^{-1} dy \\ &\leq 4\beta\kappa\mu^{-1}. \end{aligned}$$

Adding the two bounds gives the result

$$\begin{aligned} \left\| \int_0^\infty T e^{Mt} T^\dagger - e^{Nt} dt \right\| &\leq \left\| \frac{1}{2\pi i} \int_{\mathbb{R}} \frac{1}{iy} S(iy) dy \right\| \\ &\leq \frac{1}{2\pi} 8\kappa\mu^{-1}(1 + \beta). \end{aligned}$$

□

5.4 Comparing the relaxation time of N and N_0

Theorem 6. *If $\Theta\Gamma^{-1}$ is small enough then*

$$\Delta\tau_1 = \left\| \int_0^\infty e^{Nt} - e^{N_0 t} dt \right\| \leq 4\kappa\mu^{-2} \|\nu\|$$

where μ and κ can also be replaced by μ_0 and κ_0 . This gives a bound on the relative error

$$\Delta\tau_{1,\text{rel}} = \Delta\tau_1/\tau \leq 4\kappa\mu^{-1} \|\nu\| = k'_2\Theta\Gamma^{-1}$$

where k'_2 is scaling invariant.

Proof. In this case we don't need to bound the resolvent, instead we can evaluate the integral

$$\int_0^\infty e^{Nt} - e^{N_0 t} dt = N^{-1} - N_0^{-1}.$$

We use the inverse bound (15) twice. First, because $\|\nu\| \leq \frac{1}{2} \|b^{-1}\|^{-1}$ as long as $\Theta\Gamma^{-1}$ is small enough, we can apply the bound on

$$\|(b - \nu)^{-1} - b^{-1}\| \leq 2 \|b^{-1}\|^2 \|\nu\|. \quad (19)$$

Now, apply the bound again with $A = N$ and $B = N_0 - N$. The condition for B is

$$\begin{aligned}\|B\| &\leq \|a\|^2 \|(b - \nu)^{-1} - b^{-1}\| \\ &\leq \|a\|^2 2 \|b^{-1}\|^2 \|\nu\| \\ &= 2\kappa \|\nu\| \\ &\leq 2 \|A^{-1}\|^{-1} = 2\mu\end{aligned}$$

where we used (19) in the second step. The last inequality is again achieved for $\Theta\Gamma^{-1}$ small enough because the two sides scale like

$$\Theta^2\Gamma^{-2}\Theta \leq \Theta^2\Gamma^{-1}.$$

Now it follows that

$$\|N^{-1} - N_0^{-1}\| \leq 2 \|A^{-1}\|^2 \|B\| = 4\kappa\mu^{-2} \|\nu\|$$

as claimed. By switching the role of b and b_0 we receive the corresponding bound with κ_0 and μ_0 . \square

As a corollary we receive a bound on the relaxation time difference between the fully quantum mechanical evolution of M and the simple kinetic network evolution of N_0 .

Corollary 7. *If $\Theta\Gamma^{-1}$ is small enough then for some scaling independent constant k_1*

$$\Delta\tau_{0, \text{rel}} \leq k_1\Theta\Gamma^{-1}$$

Proof. According to Proposition 4 we have $|\mu - \mu_0|/\mu_0 \rightarrow 0$, and therefore there is a c such that

$$c \geq \tau/\tau_0$$

for $\Theta\Gamma^{-1}$ small enough. Then with Theorems 5 and 6 we have

$$\begin{aligned}\Delta\tau_{0, \text{rel}} &= \Delta\tau_0/\tau_0 \\ &\leq (\Delta\tau + \Delta\tau_1)/\tau_0 \\ &\leq c(\Delta\tau + \Delta\tau_1)/\tau \\ &\leq c(\Delta\tau_{\text{rel}} + \Delta\tau_{1, \text{rel}}) \\ &\leq k_1\Theta\Gamma^{-1}.\end{aligned}$$

\square

6 Bounding evolution error

In this chapter we bound the difference of time evolution operators for M , N and N_0 . Our error bounds looks as follows

$$\|e^{Mt} - e^{Nt}\| \leq e^{-\mu t/2} \cdot X$$

where X is proportional to $\Theta^2\Gamma^{-2}$ up to a logarithmic term, and proportional to $\Theta\Gamma^{-1}$ if N is replaced with N_0 . The logarithmic term appears due to intermediate times. It seems the integral over time performed in the last chapter seems to have conveniently guided us around that logarithm. As for the time dependence, using a shifting integration contour might give a bound like $e^{-\mu t}\mu t$, but a better control of the spectrum would be necessary to shift the contour close to $-\mu$ for long times.

As in the last chapter in 5.2, we write the evolution difference as a complex integral before we prove bounds

$$\|Te^{Mt}T^\dagger - e^{Nt}\| = \left\| \frac{1}{2\pi i} \oint e^{zt} S(z) dt \right\|. \quad (20)$$

Note that all the results in this Section again require the conditions in 4.2.

6.1 Comparing the evolution of M and N

We will change the contour integration in (20) to be parallel to the imaginary axis $z = iy - \mu/2$ for $y \in \mathbb{R}$. With this choice the exponential in the integral yields exponential decay at rate $\mu/2$. Again we give the technical bounds on $S(iy - \mu/2)$ in Lemma 12 in Section 8.

Theorem 8. *If $\Theta\Gamma^{-1}$ is small enough then for all $t \geq 0$ we have*

$$\|Te^{Mt}T^\dagger - e^{Nt}\| \leq e^{-\mu t} \cdot k_4\Theta^2\Gamma^{-2} (1 + k_5 \ln \Theta^{-1}\Gamma)$$

where k_4 and k_5 are a scaling independent constants.

Proof. We set the integration contour in (20) to parallel to the complex axis $z = iy - \mu/2$ for $y \in \mathbb{R}$ with y going from $-R$ to $+R$. We close the contour to the left in the half plane of negative real parts along a circle of radius R . According to Lemmas 11 and 12, $S(z)$ is bounded for $\text{Re } z \geq -\mu/2$ and hence has no poles. Therefore all the poles lie within the contour for R large enough and $\Theta\Gamma^{-1}$ small enough. As R tends to infinity the integrand behaves like $\frac{1}{z^2}e^{\text{Re } z}$ so the half-circle does not contribute to the integral. We can therefore change to complex integral to an integral in y over all of \mathbb{R}

$$\|Te^{Mt}T^\dagger - e^{Nt}\| = \left\| \frac{1}{2\pi} \int_{\mathbb{R}} e^{(iy-\mu/2)t} S(iy - \mu/2) dy \right\|.$$

Now split up the integral into three regions with $|y|$ in the intervals $[0, \mu]$, $[\mu, \hat{\alpha}]$ and $[\hat{\alpha}, +\infty)$ and then use the bounds from Lemma 12. Choose $\Theta\Gamma^{-1}$ small enough so that $\mu < \hat{\alpha}$ and use part 1 of the Lemma to bound

$$\begin{aligned} \left\| \int_0^{\mu/2} e^{(iy-\mu/2)t} S(iy - \mu/2) dy \right\| &\leq e^{-\mu t/2} \int_0^{\mu/2} 16\kappa\mu^{-2}|iy - \mu/2| dy \\ &\leq e^{-\mu t/2} 16\kappa \end{aligned}$$

and

$$\begin{aligned} \left\| \int_{\mu/2}^{\hat{\alpha}} e^{(iy-\mu/2)t} S(iy - \mu/2) dy \right\| &\leq e^{-\mu t/2} \int_{\mu/2}^{\hat{\alpha}} 4\kappa \cdot |y|^{-2} |iy - \mu/2| dy \\ &\leq e^{-\mu t/2} \int_{\mu/2}^{\hat{\alpha}} 4\kappa \cdot 2y^{-1} dy \\ &= e^{-\mu t/2} 8\kappa \ln(2\hat{\alpha}/\mu), \end{aligned}$$

and we use part 2 of the Lemma to bound

$$\begin{aligned} \left\| \int_{\hat{\alpha}}^{\infty} e^{(iy-\mu/2)t} S(iy - \mu/2) dy \right\| &\leq e^{-\mu t/2} \int_{\hat{\alpha}}^{\infty} 4|y|^{-2} \|a\|^2 (b_{\min} - \mu/2)^{-1} dy \\ &\leq e^{-\mu t/2} 4\hat{\alpha}^{-1} \|a\|^2 (b_{\min} - \mu/2)^{-1}. \end{aligned}$$

Adding the three bounds gives the result

$$\|Te^{Mt}T^\dagger - e^{Nt}\| \leq e^{-\mu t/2} 4 \left(4\kappa + 2\kappa \ln(2\hat{\alpha}/\mu) + \hat{\alpha}^{-1} \|a\|^2 (b_{\min} - \mu/2)^{-1} \right).$$

The middle term of the parenthesis has the worst scaling behavior

$$2\kappa \ln(2\hat{\alpha}/\mu) \propto \Theta^2\Gamma^{-2} \ln \Theta^{-1}\Gamma$$

while the other two terms scale like $\Theta^2\Gamma^{-2}$. Therefore there are some scaling independent constants k_4 and k_5 such that

$$\|Te^{Mt}T^\dagger - e^{Nt}\| \leq e^{-\mu t/2} \cdot k_4\Theta^2\Gamma^{-2} (1 + k_5 \ln \Theta^{-1}\Gamma).$$

□

6.2 Comparing the evolution of N and N_0

Theorem 9. *If $\Theta\Gamma^{-1}$ is small enough then for all $t \geq 0$ we have*

$$\|e^{Nt} - e^{N_0t}\| \leq e^{-\mu t/2} \cdot k'_4 \Theta\Gamma^{-1}$$

where k'_4 is scaling independent, and where μ and κ can also be replaced by μ_0 and κ_0 .

Proof. We are bounding the integral

$$\frac{1}{2\pi i} \oint e^{zt} \tilde{S}(z) dz$$

with resolvent difference

$$\tilde{S}(z) = \frac{1}{z - N} - \frac{1}{z - N_0}.$$

We use the same contour as in Proposition 8, $z = iy - \mu/2$. According to Proposition 4, all poles of $\tilde{S}(z)$ lie within this contour when $\Theta\Gamma^{-1}$ is small enough and R is large enough. Because of the e^{zt} factor and $T(z)$ tending to zero, the integral over the half-circle tends to 0 as R becomes large.

We bound $\tilde{S}(z)$ in much the same way that we bounded $S(z)$ in Lemma 12, however, the procedure is more straightforward. Set

$$X = (b - \nu)^{-1} - b^{-1},$$

because $\|\nu\| \leq \frac{1}{2} \|b^{-1}\|^{-1}$ we can use the inverse bound (15)

$$\|X\| \leq 2 \|b^{-1}\|^2 \|\nu\|.$$

Now rewrite

$$\tilde{S}(z) = (z - a^\dagger b^{-1} a)^{-1} + (z - a^\dagger b^{-1} a - a^\dagger X a)^{-1}.$$

For any z with $\operatorname{Re} z = -\mu/2$ and for $\Theta\Gamma^{-1}$ small enough we have

$$\begin{aligned} \|a^\dagger X a\| &\leq 2 \|a\|^2 \|b^{-1}\|^2 \|\nu\| \\ &\leq \frac{1}{2} \|z - a^\dagger b^{-1} a\| \end{aligned}$$

and so we can apply (15) again

$$\begin{aligned} \|\tilde{S}(z)\| &\leq 2 \|(z - a^\dagger b^{-1} a)^{-1}\|^2 \|a^\dagger X a\| \\ &\leq 4 \|(z - a^\dagger b^{-1} a)^{-1}\|^2 \kappa \|\nu\|. \end{aligned}$$

Now we apply inverse bounds (16) and (17) to receive the bounds

$$\|\tilde{S}(z)\| \leq 16\mu^{-2} \kappa \|\nu\| \tag{21}$$

$$\|\tilde{S}(z)\| \leq 4 |z|^{-2} \kappa \|\nu\| \tag{22}$$

as long as $\operatorname{Re} z = -\mu/2$.

To estimate the integral

$$\frac{1}{2\pi} \int_{\mathbb{R}} e^{(iy - \mu/2)t} T(iy - \mu/2) dy$$

we split it into the two regions $|y| \leq \mu/2$ and $|y| > \mu/2$. Use (21) to bound

$$\left\| \int_{-\mu/2}^{\mu/2} e^{(iy - \mu/2)t} \tilde{S}(iy - \mu/2) dy \right\| \leq e^{-\mu t/2} \cdot \mu \cdot 16\mu^{-2} \kappa \|\nu\|,$$

and use (22) to bound

$$2 \left\| \int_{\mu/2}^{\infty} e^{(iy - \mu/2)t} \tilde{S}(iy - \mu/2) dy \right\| \leq 2e^{-\mu t/2} \cdot 8\mu^{-1} \kappa \|\nu\|.$$

Adding the two bounds gives

$$\begin{aligned} \|e^{Nt} - e^{N_0t}\| &\leq 32e^{-\mu t/2} \mu^{-1} \kappa \|\nu\| \\ &\leq e^{-\mu t/2} \cdot k_6 \Theta \Gamma^{-1}. \end{aligned}$$

where k_6 is scaling independent. The whole proof works just as well when exchanging μ with μ_0 , κ with κ_0 giving a similar bound. \square

As a corollary we receive a bound on the decay time difference between the fully quantum mechanical evolution of M and the simple kinetic network evolution of N_0 .

Corollary 10. *If $\Theta \Gamma^{-1}$ is small enough then for all $t \geq 0$ we have*

$$\|Te^{Mt}T^\dagger - e^{N_0t}\| \leq e^{-\mu t/2} \cdot k_3 \Theta \Gamma^{-1}$$

where k_3 is a scaling independent constant.

Proof. The bound follows from Theorems 8 and 9 and the fact that

$$\Theta^2 \Gamma^{-2} \ln \Theta^{-1} \Gamma \leq \Theta \Gamma^{-1}$$

for $\Theta \Gamma^{-1} \leq 1$. \square

7 Applications

The rate of direct population exchange

$$\mu_{kl} = \frac{2|V_{kl}|^2 \gamma_{kl}}{\gamma_{kl}^2 + E_{kl}^2}$$

determines the strength of the link between sites k and l for the network N_0 . Because of our condition that $\gamma_k > 0$, the network topology is fully determined by the V_{kl} , but the strength of the links is also affected by γ_k and E_k .

As applications, we consider two idealized networks. The first is a highly connected network where all sites are linked, the second is a circular chain where only nearest neighbors are linked. We numerically calculate the relaxation times for the networks M , N_0 and N and compare the relative errors. Then we compare these networks to randomized networks with the same network topology. We also discuss the dimension dependence of our bounds from Sections 5 and again compare it to numerical simulations. All the simulations agree with our bounds, but they show much room for improvement when considering large dimensions.

Finally, we discuss the FMO-complex and our model for which some results were already shown in the introduction in Figure 1.

For clarity of notation we recall that $\Delta\tau$, $\Delta\tau_0$ and $\Delta\tau_1$ are relaxation time differences between the network pairs $M - N$, $M - N_0$ and $N - N_0$ respectively. This only makes the discussion more precise, while generally $\Delta\tau_0$ and $\Delta\tau_1$ show the same dimension and scaling behavior, with small corrections to constants.

7.1 Highly connected network

Consider a highly connected network

$$\begin{aligned} V_{kl} &= \Theta \\ E_k &= 0 \\ \gamma_k &= \Gamma. \end{aligned}$$

In Figure 2 we made a plot for the computed relative relaxation time differences $\Delta\tau_{\text{rel}}$ and $\Delta\tau_{0,\text{rel}}$ for different $\Theta \Gamma^{-1}$ with the initial state localized at site 1. Both axes plot logarithms, hence a straight line with slope n represents a $(\Theta \Gamma^{-1})^n$ proportionality.

The difference $\Delta\tau_{\text{rel}}$ is too small to show any clear behavior. The difference $\Delta\tau_{0,\text{rel}}$ is linear with slope approximately 2, hence the approximation is better than the slope 1 expected from Theorem 6. In the same figure we compare our idealized network to random networks where all V_{kl} are chosen randomly between 0 and Θ and all E_k are chosen randomly between 0 and Γ , hence they have the same topology. The magnitudes of the errors are similar for the range considered, but the slopes are different. All the samples show an error slope of 1 for $\Delta\tau_{0,\text{rel}}$, while

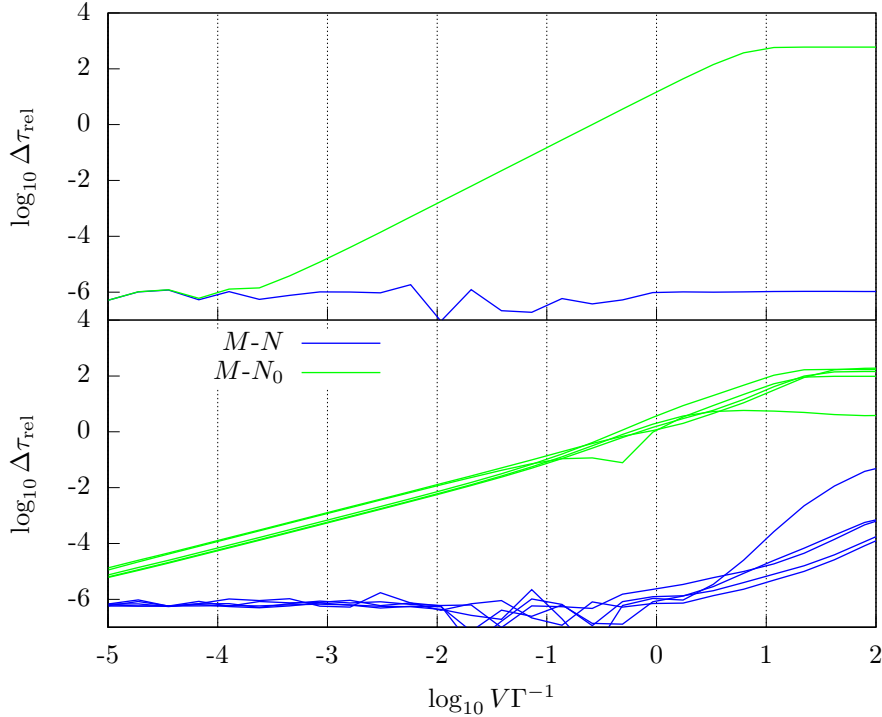


Figure 2: Relative error for the highly connected network

the error slope for $\Delta\tau_{\text{rel}}$ is varying, but in most parts steeper than the slope of $\Delta\tau_{0,\text{rel}}$. This behavior is closer to the behavior expected from our bounds. Generally, the agreement is about six orders of magnitude better for the network N than the network N_0 .

For the ideal highly connected network we derive the quantities used in Theorem 5 and 6 analytically in Appendix C. The resulting bounds are

$$\begin{aligned}\Delta\tau_{\text{rel}} &\leq c_1 n \Theta^2 \Gamma^{-2} \\ \Delta\tau_{1,\text{rel}} &\leq c_2 n \Theta \Gamma^{-1}\end{aligned}$$

for dimension and scaling independent constants c_1 and c_2 . The simulation of M has a relatively high error and becomes slow very fast as n gets larger. Hence, we can only get meaningful results for $\Delta\tau_{1,\text{rel}}$, the relaxation time difference of networks N and N_0 . The result in Figure 3 actually shows that the difference increases with slope 2 or proportional to n^2 . The reason is that in Theorem 6 we have the condition $\|\nu\| \leq \frac{1}{2} \|b^{-1}\|^{-1}$ where the LHS is proportional to n and the RHS is constant (also discussed in the Appendix). If we increase the dimension at constant scaling, this condition and our bound break down. To still get a bound for large n we would need to readjust the scaling.

7.2 Linear network

Assume the sites are positioned on a circle and only nearest neighbors interact with strength Θ

$$V_{kl} = \begin{cases} \Theta & |k-l| = 1 \\ 0 & \text{else} \end{cases}$$

where we use the equivalence $n \equiv 0$. Further $\gamma_k = \Gamma$ and E_k such that $E_{kl} = \Gamma E$ when $|k-l| = 1$ which is possible for n even.

In Figure 4 we made a plot of the computed relative relaxation time differences $\Delta\tau_{\text{rel}}$ and $\Delta\tau_{0,\text{rel}}$ for different $\Theta\Gamma^{-1}$ with the initial state localized at site 1. Interestingly the quality of approximation by N_0 is improved over the highly connected model, while the quality of approximation by N has decreased. Also, both models show the same

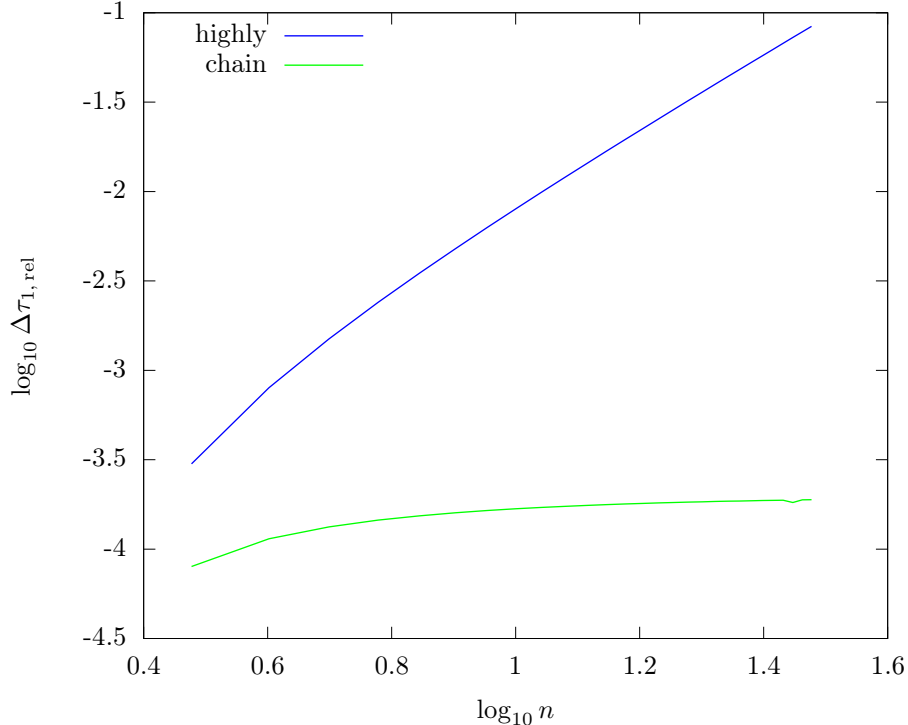


Figure 3: Relative errors between N and N_0 for the highly connected network and the cyclical chain with increasing dimension and $\Theta = 0.01$ and $\Gamma = 1$.

slope of about 2. We compare the ideal chain to random chains for which the V_{kl} that equal Θ in the idealized case are instead chosen randomly between 0 and Θ , and all E_k are chosen randomly between 0 and Γ . We get essentially the same behavior with all slopes being 2. That hints at a possible improvement of our bound in Theorem 6 in the case where the network is a chain, improving the proportionality from $\Theta\Gamma^{-1}$ to $\Theta^2\Gamma^{-2}$. Generally, the agreement is about five orders of magnitude better for the network N than the network N_0 .

As in the last section, we can derive the necessary quantities for our bounds and get

$$\begin{aligned}\Delta\tau_{\text{rel}} &\leq c_3\Theta^2\Gamma^{-2}n^2 \\ \Delta\tau_{1,\text{rel}} &\leq c_4\Theta\Gamma^{-1}n^2\end{aligned}$$

for dimension and scaling independent constants c_3 and c_4 . This time the condition $\|\nu\| \leq \frac{1}{2}\|b^{-1}\|^{-1}$ does not break down and the bounds hold for large dimensions as well. The n^2 terms are due to the lowest eigenvalue of N_0 being proportional to n^{-2} . This is a weakness of our strategy to use the operator norm for our bounds. Better bounds should be possible when only considering localized exciton as initial state. This initial state would be a superposition of all the eigenstates on N_0 , and the average relaxation time would enter the bounds, instead of the longest relaxation time (the smallest eigenvalue of N_0).

As above we skip the simulation of M because the error is too large, and consider $\Delta\tau_{1,\text{rel}}$ only. The result in Figure 3 shows that the difference seems to approximate a constant value for larger dimensions. So, both our bounds could be improved for large dimensions.

7.3 The FMO-complex

The FMO-complex is pigment-protein with trimer structure. Each monomer contains seven bacteriochlorophyll a pigments that capture and transport light. The excitons start out at site 1 or 6 and the trapping occurs at site 3 [1], we set the initial state to be

$$\vec{p}_0 = (1/2, 0, 0, 0, 0, 1/2, 0)^\dagger.$$

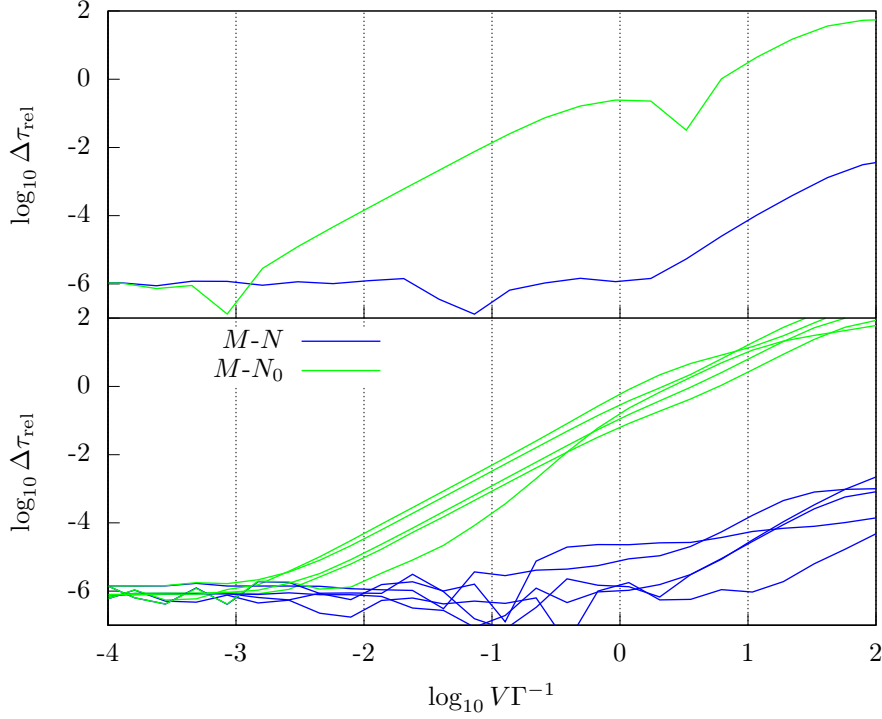


Figure 4: Relative error for the circular chain

We use the same numerical values as [11], with interactions and energies from [4]. The system Hamiltonian is

$$H + V = \begin{pmatrix} 280 & -106 & 8 & -5 & 6 & -8 & -4 \\ -106 & 420 & 28 & 6 & 2 & 13 & 1 \\ 8 & 28 & 0 & -62 & -1 & -9 & 17 \\ -5 & 6 & -62 & 175 & -70 & -19 & -57 \\ 6 & 2 & -1 & -70 & 320 & 40 & -2 \\ -8 & 13 & -9 & -19 & 40 & 360 & 32 \\ -4 & 1 & 17 & -57 & -2 & 32 & 260 \end{pmatrix}$$

with all the numbers in cm^{-1} (or $2.9978 \cdot 10^{10} s^{-1}$). Exciton recombination at rate $\kappa = 1ns^{-1}$ and reaction center trapping at rate $\kappa_3 = 1ps^{-1}$ enter the anti-hermitian operator

$$A = -\frac{i}{2} \left(\sum_k \kappa |k\rangle \langle k| + \kappa_3 |3\rangle \langle 3| \right).$$

We use the same dephasing rate for every site $\gamma_k = \gamma$, and vary γ from 10^{-3} to $10^5 cm^{-1}$. Efficiency is calculated as

$$f = \kappa_3 \int_0^\infty \rho_{33}(t) dt$$

we calculated f for the three models in Figure 1. Peak efficiency is reached for $\gamma \approx 170 cm^{-1}$ close to the average energy gap along the chain which is $146 cm^{-1}$. The approximation N has less than 1% error, even for the lowest γ used, and the approximation N_0 gets below 1% error for $\gamma \approx 2 cm^{-1}$. Comparing this to our bounds we have

$$\|a\| = \|a^\dagger\| = 215 cm^{-1}$$

and for large γ

$$\|b^{-1}\|^{-1} = \gamma.$$

The numerical factor β is changing because of the changing ratio between energies and dephasing, for large γ however it is approximately equal to 100. Hence, our bound becomes

$$\Delta\tau_{\text{rel}} \lesssim 100 (215\text{cm}^{-1}\gamma^{-1})^2.$$

The 1% error margin is reached only when $\gamma = 21500\text{cm}^{-1}$, so our numerical factors could certainly be much improved. But this is not unexpected, since our main goal was to find the leading behavior in $\Theta\Gamma^{-1}$.

We give N_0 for maximal transfer efficiency

$$N_0(\gamma = 170\text{cm}^{-1}) = \begin{pmatrix} -80 & 79 & 0 & 0 & 0 & 1 & 0 \\ 79 & -82 & 1 & 0 & 0 & 2 & 0 \\ 0 & 1 & -58 & 22 & 0 & 0 & 1 \\ 0 & 0 & 22 & -88 & 33 & 2 & 31 \\ 0 & 0 & 0 & 33 & -52 & 18 & 0 \\ 1 & 2 & 0 & 2 & 18 & -31 & 9 \\ 0 & 0 & 1 & 31 & 0 & 9 & -41 \end{pmatrix}.$$

It is interesting that the rate between sites 2 and 3 is actually smaller than the rate between sites 2 and 6 even though $|V_{23}| > |V_{26}|$. The reason is the large energy gap between sites 2 and 3 of 420cm^{-1} while sites 2 and 6 have an energy gap of 60cm^{-1} . However, the values for site energies are still up to some debate [1, 4], and small changes can easily turn this behavior to the opposite again.

8 Resolvent difference bounds

The following three Lemmas are the main technical parts of our bounds. They all consist of bounding the operator norm of the resolvent difference

$$S(z) = \frac{1}{z - a^\dagger(b - z)^{-1}a} - \frac{1}{z - a^\dagger b^{-1}a}$$

for different values of z . Conceptually the bounding procedure is simple, we only employ the inverse bounds introduced in 4.3. Loosely speaking, if $|z| < \Gamma$ we can expand $(b - z)^{-1}$ and then the two terms in $S(z)$ only have a small difference in the denominator, so, using another inverse bound, they almost cancel. If $|z| > \Gamma$ then $|z| \gg \|a^\dagger b^{-1}a\|$ and we can directly use the second step from the case $|z| < \Gamma$.

Of course we also have to keep in mind where the poles of $S(z)$ are. According to Proposition 4 $(z - N)^{-1}$ has poles on the real axis below $-\mu$ which move according to the scaling $\Theta^2\Gamma^{-1}$. On the other hand $(z - a^\dagger(b - z)^{-1}a)^{-1}$ has poles close to the poles of $(z - N)^{-1}$ that approximately cancel each other, but it also has poles close to the eigenvalues of b which are approximately $\alpha_{ij} = -\gamma_{ij} + iE_{ij}$ and $\bar{\alpha}_{ij}$, scaling like Γ . Comparing the two sets of poles, the b -poles are much further to the left (negative real values) than the N -poles because $\Gamma \gg \Theta^2\Gamma^{-1}$. Our lemma steer clear of this poles by keeping $\text{Re } z \geq -\mu/2$.

Lemma 11 contains bounds for $\text{Re } z \geq 0$ which on the one hand ensures there are no poles on the right side of the complex plane, and on the other hand we use the bounds for $z = iy$ to bound the relaxation time. Lemma 12 contains bounds for the region $-\mu/2 \leq \text{Re } z \leq 0$ the bounds are derived in a similar fashion as in Lemma 11, but there are some additional complications.

8.1 Bounds in the right half plane

Lemma 11. *If $\Theta\Gamma^{-1}$ is small enough and $\text{Re } z \geq 0$ then $S(z)$ is bounded by*

1. $\|S(z)\| \leq 4\kappa\mu^{-2}|z|$ if $|z| \leq \alpha$, where $\alpha \propto \Gamma$ depends on a and b ,
2. $\|S(z)\| \leq 4\beta\kappa|z|^{-1}$ for any z with $\text{Re } z \geq 0$, where β is a scaling independent constant depending on a and b .

Proof. 1. Assume $\text{Re } z \geq 0$ and $|z| \leq \alpha \propto \Gamma$, where

$$\alpha = \min \left\{ \frac{1}{2} \|b^{-1}\|^{-1}, \frac{1}{4}\kappa^{-1}\mu \right\}. \quad (23)$$

Set

$$X = (b - z)^{-1} - b^{-1}$$

and because $|z| \leq \frac{1}{2} \|b^{-1}\|^{-1}$ we can use (15) and have

$$\|X\| \leq 2 \|b^{-1}\|^2 |z|.$$

Rewrite

$$S(z) = (z - a^\dagger b^{-1} a - a^\dagger X a)^{-1} - (z - a^\dagger b^{-1} a)^{-1}.$$

To use (15) on this expression notice that

$$|z| \leq \frac{1}{4} \kappa^{-1} \mu$$

and therefore

$$\begin{aligned} \|a^\dagger X a\| &\leq 2\kappa |z| \\ &\leq \frac{1}{2} \mu \\ &\leq \frac{1}{2} \|(z - a^\dagger b^{-1} a)^{-1}\|^{-1} \end{aligned}$$

where (16) was applied in the last step, using the fact that $a^\dagger b^{-1} a$ is self-adjoint from Proposition 4. This is just the condition for the bound

$$\begin{aligned} \|S(z)\| &\leq 2 \|(z - a^\dagger b^{-1} a)^{-1}\|^2 \|a^\dagger X a\| \\ &\leq 4\kappa \|(z - a^\dagger b^{-1} a)^{-1}\|^2 |z| \end{aligned}$$

again using (16) and also (17) we get the bounds

$$\begin{aligned} \|S(z)\| &\leq 4\kappa \mu^{-2} |z| \\ \|S(z)\| &\leq 4\kappa |z|^{-1} \end{aligned} \tag{24}$$

for $|z| \leq \alpha$. The first bound is bound 1 of the Lemma, the second bound will be used below.

2. We now derive a bound when $|z| \geq \alpha$ and $\operatorname{Re} z \geq 0$, we will combine it with (24) to receive bound 2 for all $z \in \mathbb{R}$. If $\Theta\Gamma^{-1}$ is small enough then we have

$$\begin{aligned} \|a^\dagger b^{-1} a\| &\leq \frac{\alpha}{2} \leq \frac{1}{2} |z| \\ \|a^\dagger (b - z)^{-1} a\| &\leq \frac{\alpha}{2} \leq \frac{1}{2} |z|. \end{aligned}$$

Where the latter inequality uses the fact that the spectrum of b approaches the spectrum of b_0 as $\Theta\Gamma^{-1}$ becomes small, and the spectrum of b_0 , which is $-\gamma_{ij} \pm iE_{ij}$, has negative real part $-\gamma_{ij} < 0$. The last two inequalities are the conditions to use (15) and get the two bounds

$$\begin{aligned} \|(z - a^\dagger (b - z)^{-1} a)^{-1} - z^{-1}\| &\leq 2|z|^{-2} \|a^\dagger (b - z)^{-1} a\| \\ \|(z - a^\dagger b^{-1} a)^{-1} - z^{-1}\| &\leq 2|z|^{-2} \|a^\dagger b^{-1} a\| \end{aligned}$$

set

$$b_{\min} = \min \{|\operatorname{Re} \lambda| \mid \lambda \in \operatorname{Spec} b\} \propto \Gamma \tag{25}$$

the closest any eigenvalue of b gets to the imaginary axis. Then $\|b^{-1}\| \leq b_{\min}^{-1}$ and $\|(b - z)^{-1}\| \leq b_{\min}^{-1}$ so

$$\|S(z)\| \leq 4|z|^{-2} \|a\|^2 d^{-1}.$$

Comparing to (24) with

$$\beta = \max \left\{ 1, 1 / \left(\alpha b_{\min} \|b^{-1}\|^2 \right) \right\} \propto 1$$

we have

$$4|z|^{-2} \|a\|^2 b_{\min}^{-1} \leq \beta \cdot 4\kappa |z|^{-1}$$

for $|z| \geq \alpha$ and therefore

$$\|S(z)\| \leq 4\beta\kappa |z|^{-1} \tag{26}$$

for all z with $\operatorname{Re} z \geq 0$. Which is bound 2 of the Lemma. \square

8.2 Bounds parallel to the imaginary axis

The following Lemma establishes bounds along the imaginary axis $z = iy - \tilde{\mu}$. These bounds are used to prove the evolution bounds.

Lemma 12. *If we choose $\Theta\Gamma^{-1}$ small enough then for $0 \leq \tilde{\mu} \leq \mu/2$ the resolvent difference $S(iy - \tilde{\mu})$ is bounded by*

1. $\|S(iy - \tilde{\mu})\| \leq 16\kappa\mu^{-2}|iy - \tilde{\mu}|$ and $\|S(iy - \tilde{\mu})\| \leq 4\kappa|y|^{-2}|iy - \tilde{\mu}|$ if $|y| \leq \hat{\alpha}$, where $\hat{\alpha} \propto \Gamma$ depends on a and b ,
2. $\|S(y)\| \leq 4|y|^{-2}\|a\|^2(b_{\min} - \tilde{\mu})^{-1}$ for $|y| > \hat{\alpha}$ with $b_{\min} \propto \Gamma$.

Proof. We proceed almost identically as in the proof of Lemma 11 using the inverse bounds 15, (16) and (17) for the same parts of the resolvent terms.

1. We use the α from (23) to define

$$\hat{\alpha} = \min \left\{ \frac{1}{2} \|b^{-1}\|^{-1}, \frac{1}{8}\kappa^{-1}\mu \right\} - \mu$$

notice that the scaling $\hat{\alpha} \propto \Gamma$ is only approximate and that $\Theta\Gamma^{-1}$ needs to be small enough such that $\hat{\alpha} > 0$. Now require $|y| \leq \hat{\alpha} \propto \Gamma$. Set

$$X = (b - iy + \tilde{\mu})^{-1} - b^{-1}$$

and because we have

$$\begin{aligned} |iy - \tilde{\mu}| &\leq |y| + \tilde{\mu} \\ &\leq \frac{1}{2} \|b^{-1}\|^{-1} - \mu + \tilde{\mu} \\ &\leq \frac{1}{2} \|b^{-1}\|^{-1} \end{aligned}$$

we can use (15) to get the bound

$$\|X\| \leq 2 \|b^{-1}\|^2 |iy - \tilde{\mu}|.$$

Rewrite

$$S(iy - \tilde{\mu}) = (iy - \tilde{\mu} - a^\dagger b^{-1} a - a^\dagger X a)^{-1} - (iy - \tilde{\mu} - a^\dagger b^{-1} a)^{-1}.$$

To use (15) on this expression notice that we have

$$\begin{aligned} |iy - \tilde{\mu}| &\leq |y| + \tilde{\mu} \\ &\leq \left(\frac{1}{8}\kappa^{-1}\mu - \mu \right) + \tilde{\mu} \\ &\leq \frac{1}{8}\kappa^{-1}\mu \end{aligned}$$

and therefore

$$\begin{aligned} \|a^\dagger X a\| &\leq 2\kappa |iy - \tilde{\mu}| \\ &\leq \frac{1}{4}\mu \\ &\leq \frac{1}{2} \|(iy - \tilde{\mu} - a^\dagger b^{-1} a)^{-1}\|^{-1} \end{aligned}$$

where (16) was applied in the last step, using the fact that $\tilde{\mu} + a^\dagger b^{-1} a \leq -\mu/2$ from Proposition 4. This is just the condition for the bound

$$\begin{aligned} \|S(iy - \tilde{\mu})\| &\leq 2 \|(iy - \tilde{\mu} - a^\dagger b^{-1} a)^{-1}\|^2 \|a^\dagger X a\| \\ &\leq 4\kappa \|(iy - \tilde{\mu} - a^\dagger b^{-1} a)^{-1}\|^2 |iy - \tilde{\mu}| \end{aligned}$$

again using (16) and also (17) we get the bounds

$$\begin{aligned}\|S(iy - \tilde{\mu})\| &\leq 16\kappa\mu^{-2}|iy - \tilde{\mu}| \\ \|S(iy - \tilde{\mu})\| &\leq 4\kappa|y|^{-2}|iy - \tilde{\mu}|\end{aligned}$$

for $|y| \leq \hat{\alpha}$. These are the bounds in part 1 of our Lemma.

2. We now derive a bound when $|y| \geq \hat{\alpha}$. If $\Theta\Gamma^{-1}$ is small enough then

$$\begin{aligned}\|a^\dagger b^{-1} a + \tilde{\mu}\| &\leq \frac{\hat{\alpha}}{2} \leq \frac{1}{2}|y| \\ \|a^\dagger (b - iy + \tilde{\mu})^{-1} a + \tilde{\mu}\| &\leq \frac{\hat{\alpha}}{2} \leq \frac{1}{2}|y|.\end{aligned}$$

The last two inequalities are the conditions to use (15) and get the two bounds

$$\begin{aligned}\|(iy - \tilde{\mu} - a^\dagger (b - iy + \tilde{\mu})^{-1} a)^{-1} - (iy - \tilde{\mu})^{-1}\| &\leq 2|y|^{-2} \|a^\dagger (b - iy + \tilde{\mu})^{-1} a\| \\ \|(iy - \tilde{\mu} - a^\dagger b^{-1} a)^{-1} - (iy - \tilde{\mu})^{-1}\| &\leq 2|y|^{-2} \|a^\dagger b^{-1} a\|.\end{aligned}$$

Use b_{\min} from (25), giving

$$\begin{aligned}\|(b - iy + \tilde{\mu})^{-1}\| &\leq (b_{\min} - \tilde{\mu})^{-1} \\ \|(b - iy + \tilde{\mu})^{-1}\| &\leq (b_{\min} - \tilde{\mu})^{-1}\end{aligned}$$

and so

$$\|S(iy - \tilde{\mu})\| \leq 4|y|^{-2} \|a\|^2 (b_{\min} - \tilde{\mu})^{-1}.$$

for $|y| > \hat{\alpha}$, which is the bound in part 2 of our Lemma. \square

9 Conclusion

We studied kinetic networks that approximate the energy transfer in a quantum network subject to dephasing. The first network N_0 derives its rates only from nearest neighbor interactions, while the second N includes higher order corrections. We proved that the relaxation times are proportional to $\Theta\Gamma^{-1}$ and $\Theta^2\Gamma^{-2}$ respectively. Hence, the approximations are good if the interaction gets weak, or the dephasing and/or energy gaps get large. In the case of the FMO complex, both kinetic networks are good approximations in the regime of dephasing-assisted energy transfer. With simulations we found that the more complex kinetic network N provides approximations with a percentage error 5-6 magnitudes smaller than the simple kinetic network.

The study of these approximations could be extended in several ways. First, one could study the higher order corrections involved in N . Second, when the interactions V_{kl} are complex, N can be non-symmetric, meaning population exchange between sites is directed, this might relate to coherent cancellations along loops as mentioned in [3]. And finally, it would be interesting how our method of splitting population and coherence space to achieve kinetic network approximations could be generalized to other quantum networks and how it relates to existing models to approximate coherent evolution with incoherent statistical evolution.

10 Acknowledgments

I want to thank Chris King for his support, ideas and many useful discussions.

A Three sites

In the following we write out parts of the master equation (3) for the case $n = 3$ and then derive the form of the matrix M . Then we explain how to generalize that form to higher n . For simplicity of notation we omit the scaling factors Γ and Θ , until we reach a block matrix expression. First note that with a standard calculation one finds $\mathcal{L}(\rho)$ to decrease the coherences in the manner

$$(\mathcal{L}(\rho))_{kl} = -\gamma_{kl}\rho_{kl}$$

where $k \neq l$ and $\gamma_{kl} = \frac{1}{2}(\gamma_k + \gamma_l)$ and $(\mathcal{L}(\rho))_{kk} = 0$. This gives a diagonal contribution $-\gamma_{kl}$ in the diagonal of the two rows corresponding to the real and imaginary part of ρ_{kl} .

Now, we evaluate the commutator

$$\left[\begin{pmatrix} E_1 & V_{12} & V_{13} \\ V_{21} & E_2 & V_{23} \\ V_{31} & V_{32} & E_3 \end{pmatrix}, \begin{pmatrix} \rho_{11} & \rho_{12} & \rho_{13} \\ \rho_{21} & \rho_{22} & \rho_{23} \\ \rho_{31} & \rho_{32} & \rho_{33} \end{pmatrix} \right].$$

From the 1x1 entry we get

$$\begin{aligned} \dot{\rho}_{11} &= -i(E_1\rho_{11} + V_{12}\rho_{21} + V_{13}\rho_{31} - E_1\rho_{11} - V_{21}\rho_{12} - V_{31}\rho_{13}) \\ &= -i(V_{12}\bar{\rho}_{12} + V_{13}\bar{\rho}_{13} - \bar{V}_{12}\rho_{12} - \bar{V}_{13}\rho_{13}) \\ &= 2 \operatorname{Im}(V_{12}\bar{\rho}_{12} + V_{13}\bar{\rho}_{13}) \\ &= 2(-V_{12}^r\rho_{12}^i + V_{12}^i\rho_{12}^r - V_{13}^r\rho_{13}^i + V_{13}^i\rho_{13}^r) \end{aligned}$$

where superscripts r and i are shortcuts for real and imaginary parts, and from the 1x2 entry we get

$$\begin{aligned} \dot{\rho}_{12} &= -i(E_1\rho_{12} + V_{12}\rho_{22} + V_{13}\rho_{32} - V_{12}\rho_{11} - E_2\rho_{12} - V_{32}\rho_{13}) - \gamma_{12}\rho_{12} \\ &= -i((E_1 - E_2)\rho_{12} + V_{12}\rho_{22} - V_{12}\rho_{11} + V_{13}\bar{\rho}_{23} - \bar{V}_{23}\rho_{13}) - \gamma_{12}\rho_{12} \end{aligned}$$

with real and imaginary parts

$$\begin{aligned} \dot{\rho}_{12}^r &= -V_{12}^i\rho_{11}^r + V_{12}^i\rho_{22}^r - \gamma_{12}\rho_{12}^r + (E_1 - E_2)\rho_{12}^r + V_{23}^i\rho_{13}^r - V_{23}^r\rho_{13}^i + V_{13}^i\rho_{23}^r - V_{13}^r\rho_{23}^i \\ \dot{\rho}_{12}^i &= V_{12}^r\rho_{11}^i - V_{12}^r\rho_{22}^i - (E_1 - E_2)\rho_{12}^i - \gamma_{12}\rho_{12}^i + V_{23}^r\rho_{13}^i + V_{23}^i\rho_{13}^r - V_{13}^r\rho_{23}^i - V_{13}^i\rho_{23}^r. \end{aligned}$$

From these results we can read off lines 1, 4 and 5 of the following matrix and fill in the remaining lines in the same fashion

$$M = \begin{pmatrix} 0 & \sqrt{2}V_{12}^i & -\sqrt{2}V_{12}^r & \sqrt{2}V_{13}^i & -\sqrt{2}V_{13}^r & \sqrt{2}V_{23}^i & -\sqrt{2}V_{23}^r \\ -\sqrt{2}V_{12}^i & \sqrt{2}V_{12}^r & -\sqrt{2}V_{12}^i & -\sqrt{2}V_{13}^i & \sqrt{2}V_{13}^r & -\sqrt{2}V_{23}^i & \sqrt{2}V_{23}^r \\ \sqrt{2}V_{12}^i & -\sqrt{2}V_{12}^r & -\gamma_{12} & E_{12} & V_{23}^i & -V_{23}^r & V_{13}^i & -V_{13}^r \\ -\sqrt{2}V_{13}^i & \sqrt{2}V_{13}^r & -E_{12} & -\gamma_{12} & V_{23}^i & V_{23}^r & -V_{13}^i & -V_{13}^r \\ \sqrt{2}V_{13}^i & -\sqrt{2}V_{13}^r & -V_{23}^i & -V_{23}^r & -\gamma_{13} & E_{13} & V_{12}^i & V_{12}^r \\ -\sqrt{2}V_{23}^i & \sqrt{2}V_{23}^r & V_{23}^i & -V_{23}^r & -E_{13} & -\gamma_{13} & -V_{12}^i & V_{12}^r \\ \sqrt{2}V_{23}^i & -\sqrt{2}V_{23}^r & -V_{13}^i & V_{13}^r & -V_{12}^i & V_{12}^r & -\gamma_{23} & E_{23} \\ -\sqrt{2}V_{23}^i & \sqrt{2}V_{23}^r & V_{13}^i & V_{13}^r & -V_{12}^i & -V_{12}^r & -E_{23} & -\gamma_{23} \end{pmatrix}$$

where we define $E_{ij} = E_i - E_j$. Written as a block matrix

$$M = \begin{pmatrix} 0 & -a^\dagger \\ a & b \end{pmatrix}$$

one can see the explicit form of the matrices a , and b . Remember that we also separated b into two parts. We set the 2x2-block diagonal that scales like Γ (the E_{ij} and γ_{ij} entries) to be b_0 and we set the block-off-diagonal that scales like Θ (all the V_{ij} entries) to be ν . So $b = b_0 + \nu$.

In 3.3 in (8) we defined a transformation U to diagonalize b_0 , if we extend this transformation to the entire space $P \oplus C$ as

$$\hat{U} = \mathbb{1}_n \oplus U$$

we can apply it to M directly and get

$$\tilde{M} = \hat{U}^\dagger M \hat{U} = \begin{pmatrix} 0 & -V_{12} & -\bar{V}_{12} & -V_{13} & -\bar{V}_{13} & -V_{23} & -\bar{V}_{23} \\ -V_{12} & \bar{V}_{12} & -V_{13} & \bar{V}_{13} & -V_{23} & \bar{V}_{23} \\ \bar{V}_{12} & -\bar{V}_{12} & \alpha_{12} & -iV_{23} & -i\bar{V}_{13} & -i\bar{V}_{13} \\ V_{12} & -V_{12} & \alpha_{12} & \bar{\alpha}_{12} & i\bar{V}_{23} & iV_{13} \\ \bar{V}_{13} & -\bar{V}_{13} & -i\bar{V}_{23} & \alpha_{13} & \bar{\alpha}_{13} & i\bar{V}_{12} \\ V_{13} & -V_{13} & iV_{23} & \bar{\alpha}_{13} & -iV_{12} \\ \bar{V}_{23} & -\bar{V}_{23} & i\bar{V}_{13} & iV_{12} & \alpha_{23} \\ V_{23} & -V_{23} & -iV_{13} & -i\bar{V}_{12} & \bar{\alpha}_{23} \end{pmatrix}$$

row	column	entry	row	column	entry
kl	km	$-iV_{lm}$	\overline{kl}	\overline{km}	$i\overline{V}_{lm}$
lk	mk	iV_{lm}	\overline{lk}	\overline{mk}	$-i\overline{V}_{lm}$
lk	\overline{km}	$-iV_{lm}$	\overline{lk}	km	iV_{lm}

Table 1: The non-zero entries of $\tilde{\nu}$, always $l \neq m$

where $\alpha_{ij} = -\gamma_{ij} + iE_{ij}$. This new matrix consists of the matrices \tilde{a} and \tilde{b}_0 also introduced in 3.3

$$\tilde{M} = \begin{pmatrix} 0 & -\tilde{a}^\dagger \\ \tilde{a} & \tilde{b} \end{pmatrix}$$

where

$$\begin{aligned} \tilde{b} &= U^\dagger b U \\ &= \tilde{b}_0 + \tilde{\nu} \end{aligned}$$

with $\tilde{\nu} = U^\dagger \nu U$. The two kinetic networks are

$$\begin{aligned} N_0 &= \tilde{a}^\dagger \tilde{b}_0^{-1} \tilde{a} \\ N &= \tilde{a}^\dagger \tilde{b}^{-1} \tilde{a} \end{aligned}$$

which also holds with all the tildes removed.

It is straightforward to generalize the matrices \tilde{a} and \tilde{b}_0 to $n > 3$. Matrix \tilde{a} connects the population of site k to the coherences between site k and any other site l with strength V_{kl} , and matrix \tilde{b}_0 is a diagonal matrix with entries α_{ij} and $\overline{\alpha}_{ij}$. A bit more complicated is the matrix $\tilde{\nu}$ it is described in the next subsection.

B General construction

Here we give a description of how to find \tilde{a} , \tilde{b}_0 and $\tilde{\nu}$ for general n . We number the n dimensions of population space P with k where $k = 1, 2, \dots, n$ and the $(n^2 - n)$ dimensions of coherence space C with kl and \overline{kl} where $k < l$ are numbers from 1 to n . According to the order defined in 2.2 the first few dimensions of C are called 12, $\overline{12}$, 13, ..., 23, $\overline{23}$, 24, etc. .

B.1 Constructing \tilde{a} and \tilde{b}_0

Matrix \tilde{a} is an $n \times (n^2 - n)$ complex matrix, with the only nonzero entries

$$\begin{aligned} \tilde{a}_{k,kl} &= \overline{V}_{kl} = -\tilde{a}_{k,lk} \\ \tilde{a}_{k,\overline{kl}} &= V_{kl} = -\tilde{a}_{k,\overline{lk}}, \end{aligned}$$

hence in every column there are only $(n - 1)$ nonzero entries.

Matrix \tilde{b}_0 is diagonal with entries

$$\begin{aligned} \left(\tilde{b}_0\right)_{kl,kl} &= -\gamma_{kl} + iE_{kl} \\ \left(\tilde{b}_0\right)_{\overline{kl},\overline{kl}} &= -\gamma_{kl} - iE_{kl}. \end{aligned}$$

B.2 Constructing $\tilde{\nu}$

The matrix $\tilde{\nu} = U^\dagger \nu U$ for any n is a somewhat complicated pattern of entries V_{kl} , signs and complex conjugates. It connects coherences between sites k and l with coherences between sites k and m with the strength V_{lm} . Entries of $\tilde{\nu}$ are only non-zero if one number of the two double indices match with further conditions on their conjugation. Table 1 shows the rules for the nonzero entries.

C Calculations for applications

C.1 Highly connected network

Assume all sites are equally interacting, and have the same energies and dephasing rates

$$\begin{aligned} V_{kl} &= \Theta \\ E_k &= 0 \\ \gamma_k &= \Gamma. \end{aligned}$$

Then every column in a has $2(n-1)$ non-zero entries all equal to Θ . A simple calculation shows that

$$a^\dagger a = 2n\Theta^2 (\mathbb{1}_n - n\vec{e}\vec{e}^\dagger)$$

so for any $\vec{v} \in I$ we have $a^\dagger a \vec{v} = 2\Theta^2 n \vec{v}$, hence

$$\|a\| = \sqrt{2n}\Theta.$$

Obviously, $b = -\Gamma \mathbb{1}_C$ and $\|b_0^{-1}\| = \Gamma^{-1}$. This gives $\kappa = 2n\Theta^2 \Gamma^{-2}$. Because

$$a^\dagger b_0^{-1} a = -\Gamma^{-1} a^\dagger a$$

we have $\mu_0 = 2n\Theta^2 \Gamma^{-1}$. Using $\mu \approx \mu_0$ we find

$$\begin{aligned} \alpha &= \min \left\{ \frac{1}{2} \|b^{-1}\|^{-1}, \frac{1}{4} \kappa^{-1} \mu \right\} \\ &= \min \left\{ \frac{1}{2} \Gamma, \frac{1}{4} \frac{2n\Theta^2 \Gamma^{-1}}{2n\Theta^2 \Gamma^{-2}} \right\} \\ &= \Gamma/4 \end{aligned}$$

and so

$$\begin{aligned} \beta &= \max \left\{ 1, \alpha^{-1} \|b^{-1}\|^{-1} \right\} \\ &= 4 \end{aligned}$$

and with Theorem 5 we get the bounds

$$\begin{aligned} \Delta\tau &\leq \frac{20}{\pi} \Gamma^{-1} \\ \Delta\tau_{\text{rel}} &\leq \frac{40}{\pi} n\Theta^2 \Gamma^{-2}. \end{aligned}$$

To get the bound on $\Delta\tau_{1,\text{rel}}$ we also estimate $\|\nu\|$, we use the fact that each column and row of ν has $(n-2)$ nonzero entries and so

$$\|\nu\| \geq vn\Theta$$

for a scaling and dimension independent constant v . Then Theorem 6 gives the bound

$$\Delta\tau_{1,\text{rel}} \leq 4vn\Theta \Gamma^{-1}.$$

The condition for this bound is

$$\|\nu\| \leq \frac{1}{2} \|b^{-1}\|^{-1}$$

the LHS is bounded from below by $vn\Theta$ and the RHS is constant, so the condition does not hold for large n .

C.2 Circular chain

Assume the sites are positioned on a circle and only nearest neighbors interact with strength Θ

$$V_{kl} = \begin{cases} \Theta & |k-l| = 1 \\ 0 & \text{else} \end{cases}$$

where we set equivalence $n \equiv 0$. Further $\gamma_k = \Gamma$ and E_k such that $E_{kl} = \Gamma E$ when $|k-l| = 1$ which is possible for n even.

Now, the column for site k in a has only 4 entries, two each for the coherences with $k-1$ and $k+1$. We calculate

$$(a^\dagger a)_{kl} = \begin{cases} 4\Theta^2 & k=l \\ -2\Theta^2 & |k-l|=1 \\ 0 & \text{else} \end{cases}$$

So $\|a^\dagger a\| = 8\Theta^2$ and $\|a\| = \sqrt{8}\Theta$, in particular there is no n dependency. Also $\|b_0^{-1}\| = 1/\sqrt{\Gamma^2 + \Gamma^2 E^2}$ and so $\kappa = \frac{8}{1+E^2}\Theta^2\Gamma^{-2}$. We have

$$N_0 = \begin{cases} -\frac{4\Theta^2}{\Gamma(1+E^2)} & k=l \\ \frac{2\Theta^2}{\Gamma(1+E^2)} & |k-l|=1 \\ 0 & \text{else} \end{cases}$$

which has the spectrum

$$\lambda_p = -\frac{4\Theta^2}{\Gamma(1+E^2)} \left(1 - \cos\left(\frac{2\pi p}{n}\right)\right) \quad (27)$$

with $p = 1 \dots n$. The nonzero eigenvalue smallest in magnitude is μ_0 , so for large n and small $\Theta\Gamma^{-1}$, approximately

$$\mu \approx \mu_0 \approx \frac{2\Theta^2}{\Gamma(1+E^2)} \left(\frac{2\pi}{n}\right)^2$$

so $\alpha = \frac{1}{16}\Gamma\left(\frac{2\pi}{n}\right)^2$ and

$$\begin{aligned} \beta &= \frac{16\Gamma\sqrt{1+E^2}}{\Gamma\left(\frac{2\pi}{n}\right)^2} \\ &= \left(\frac{2n}{\pi}\right)^2 \sqrt{1+E^2}. \end{aligned}$$

Moving the numbers into constants k_1 and k_2 , and dropping the 1 in $1 + \beta$ (fine for large n), we have

$$\begin{aligned} \Delta\tau &\leq k_1\sqrt{1+E^2}\Gamma^{-1}n^4 \\ \Delta\tau_{\text{rel}} &\leq \frac{k_2}{\sqrt{1+E^2}}\Theta^2\Gamma^{-2}n^2. \end{aligned}$$

We again estimate $\|\nu\|$, now each column and row of ν has 2 or 4 nonzero entries and so

$$v_1\Theta \leq \|\nu\| \leq v_2\Theta$$

for some scaling and dimension independent constants v_1 and v_2 . Then Theorem 6 gives the bound

$$\Delta\tau_{1, \text{rel}} \leq \frac{4}{\pi^2}v_2n^2\Theta\Gamma^{-1}.$$

This time the condition

$$\|\nu\| \leq \frac{1}{2}\|b^{-1}\|^{-1}$$

does not break down for large dimensions, so the bound holds for all n when Θ and Γ are kept constant.

References

- [1] Julia Adolphs and Thomas Renger. How proteins trigger excitation energy transfer in the FMO complex of green sulfur bacteria. *Biophysical Journal*, 91(8):2778–2797, October 2006. PMID: 16861264 PMCID: 1578489.
- [2] T. Banachiewicz. Zur berechnung der determinanten, wie auch der inversen und zur darauf basierten auflösung der systeme linearer gleichungen. *Acta Astronom. Ser. C*, 3:41–67, 1937.
- [3] Jianshu Cao and Robert J. Silbey. Optimization of exciton trapping in energy transfer processes. *The Journal of Physical Chemistry A*, 113:13825–13838, December 2009.
- [4] Minhaeng Cho, Harsha M. Vaswani, Tobias Brixner, Jens Stenger, and Graham R. Fleming. Exciton analysis in 2D electronic spectroscopy. *The Journal of Physical Chemistry B*, 109:10542–10556, June 2005.
- [5] Robert M. Clegg, Melih Sener, and Govindjee. From förster resonance energy transfer to coherent resonance energy transfer and back. pages 75610C–75610C–21, 2010.
- [6] Gregory S. Engel, Tessa R. Calhoun, Elizabeth L. Read, Tae-Kyu Ahn, Tomas Mancal, Yuan-Chung Cheng, Robert E. Blankenship, and Graham R. Fleming. Evidence for wavelike energy transfer through quantum coherence in photosynthetic systems. *Nature*, 446(7137):782–786, April 2007.
- [7] Stephan Hoyer, Mohan Sarovar, and K Birgitta Whaley. Limits of quantum speedup in photosynthetic light harvesting. *New Journal of Physics*, 12:065041, June 2010.
- [8] Akihito Ishizaki, Tessa R. Calhoun, Gabriela S. Schlau-Cohen, and Graham R. Fleming. Quantum coherence and its interplay with protein environments in photosynthetic electronic energy transfer. *Phys. Chem. Chem. Phys.*, 12(27):7319–7337, June 2010.
- [9] G. Panitchayangkoon, D. Hayes, K.A. Fransted, J.R. Caram, E. Harel, J. Wen, R.E. Blankenship, and G.S. Engel. Long-lived quantum coherence in photosynthetic complexes at physiological temperature. *Proceedings of the National Academy of Sciences*, 107(29):12766, 2010.
- [10] M B Plenio and S F Huelga. Dephasing-assisted transport: quantum networks and biomolecules. *New Journal of Physics*, 10:113019, November 2008.
- [11] P. Rebentrost, M. Mohseni, I. Kassal, S. Lloyd, and A. Aspuru-Guzik. Environment-assisted quantum transport. *New Journal of Physics*, 11:033003, 2009.
- [12] G.D. Scholes. Quantum-coherent electronic energy transfer: Did nature think of it first? *The Journal of Physical Chemistry Letters*, 1(1):2–8, 2010.
- [13] C.Y. Wong, H. Hossein-Nejad, C. Curutchet, and G.D. Scholes. Quantum-Coherent energy transfer in marine algae at ambient temperature via ultrafast photon echo studies. In *International Conference on Ultrafast Phenomena*, 2010.
- [14] Fuzhen Zhang. *The Schur complement and its applications*. Springer, 2005.